7-10-2015

Mini-ISES identifies promising carbafructopyranose-based salens for asymmetric catalysis: Tuning ligand shape via the anomeric effect

Kannan R. Karukurichi
University of Nebraska - Lincoln

Xiang Fei
University of Nebraska - Lincoln

Robert A. Swyka
University of Nebraska - Lincoln, rswyka2@unl.edu

Sylvain Broussy
University of Nebraska-Lincoln, sylvain.broussy@parisdescartes.fr

Weijun Shen
University of Nebraska - Lincoln

See next page for additional authors

Authors
Kannan R. Karukurichi, Xiang Fei, Robert A. Swyka, Sylvain Broussy, Weijun Shen, Sangeeta Dey, Sandip K. Roy, and David B. Berkowitz

PHYSICAL SCIENCES

10.1126/sciadv.1500066

Mini-ISES identifies promising carbafructopyranose-based salens for asymmetric catalysis: Tuning ligand shape via the anomeric effect

Kannan R. Karukurichi, Xiang Fei, Robert A. Swyka, Sylvain Broussy, Weijun Shen, Sangeeta Dey, Sandip K. Roy, David B. Berkowitz*

This study introduces new methods of screening for and tuning chiral space and in so doing identifies a promising set of chiral ligands for asymmetric synthesis. The carbafructopyranosyl-1,2-diamine(s) and salens constructed therefrom are particularly compelling. It is shown that by removing the native anomeric effect in this ligand family, one can tune chiral ligand shape and improve chiral bias. This concept is demonstrated by a combination of (i) x-ray crystallographic structure determination, (ii) assessment of catalytic performance, and (iii) consideration of the anomeric effect and its underlying dipolar basis. The title ligands were identified by a new mini version of the in situ enzymatic screening (ISES) procedure through which catalyst-ligand combinations are screened in parallel, and information on relative rate and enantioselectivity is obtained in real time, without the need to quench reactions or draw aliquots. Mini-ISES brings the technique into the nanomole regime (200 to 350 nmol catalyst/20 μl organic volume) commensurate with emerging trends in reaction development/process chemistry. The best-performing β-D-carbafructopyranosyl-1,2-diamine–derived salen ligand discovered here outperforms the best known organometallic and enzymatic catalysts for the hydrolytic kinetic resolution of 3-phenylpropylene oxide, one of several substrates examined for which the ligand is "matched." This ligand scaffold defines a new swath of chiral space, and anomeric effect tunability defines a new concept in shaping that chiral space. Both this ligand set and the anomeric shape-tuning concept are expected to find broad application, given the value of chiral 1,2-diamines and salens constructed from these in asymmetric catalysis.

INTRODUCTION

As part of a program directed at streamlining the process for discovering useful new reactivity and for identifying useful catalytic ligand-metal combinations, we have been laying the groundwork for an in situ enzymatic screening (ISES) approach to reaction screening. Although it is clear that reaction development requires a balance between screening and hypothesis-driven or computational (*1*, *2*) approaches, in looking for fundamentally new reactivity, a broad initial screen can be of great use. This point is underscored through the recent successes of the groups of MacMillan (*3*) and Hartwig (*4*) in exploratory screens to "accelerate serendipity" yielding amine α-arylation, and Cu-mediated alkyne hydroamination transformations, respectively, and Chirik's identification of an earth-abundant Co system for asymmetric alkene hydrogenation (*5*). Beyond this, recent advances in multicomponent reactions highlight the payoff attainable in systems with additional reactants (*6*–*8*) or catalytic entities (*9*–*13*). In such endeavors, once reactivity space is better defined, Sigman has shown that one may be able to tune the transformation, for example, by using empirical "sterimol" parameters (*14*).

The desire to interrogate catalyst structure/reactivity space broadly has spurred a parallel innovation in catalyst screening technology (*15*, *16*). On-bead catalyst libraries have been exploited to enhance throughput with readouts including infrared thermography (*17*, *18*) and gel-zone fluorescence (*19*, *20*). More recently, microfluidic approaches have been invoked to address throughput (*21*–*23*). Optical sensing methods continue to be invoked and include fluorescence resonance energy transfer (*24*), indicator-displacement assays (*16*, *25*), substrate chromophore induction (*26*), and optical rotatory dispersion (*27*). Mass spectrometric methods have proven invaluable to enhance throughput (*4*, *28*) and provide information on reactivity (*29*) and stereoselectivity (*30*, *31*). Perhaps inspired by the "combinatorial" path by which polypeptide catalysts evolve in nature, a number of successful "evolved" small-molecule catalysts feature peptidomimetic elements (*32*–*40*), perhaps none more strikingly than the catalyst suite developed by Miller and co-workers (*41*–*44*). Conversely, given both the inherent ability of enzymes to both differentiate stereoisomers and the opportunity to potentially leverage spectroscopic signals associated with a number of enzymatic transformations, we (*45*–*51*) and others (*52*–*60*) have developed protein-based sensing methods to facilitate the combinatorial catalysis enterprise.

Described herein is a miniaturized version of ISES (*47*) that is inspired by the recent disclosure from the Merck Process Group of a synthesis optimization platform that reduces volumes and quantities dramatically, down to the nanomole, for high-throughput chemistry development (*61*), by taking advantage of robotic instrumentation (*62*, *63*). This report demonstrates proof of principle of mini-ISES, by using an ultraviolet (UV)/visible (vis) spectrophotometer outfitted with a quartz micromulticell for the biphasic catalyst screening method, thereby reducing the amount of catalyst needed per screen to the level of 200 to 350 nmol. This is done without specialized equipment, setting the stage for much higher-throughput, robotic versions of the technique, by demonstrating that catalysts can be effectively characterized from the reporting enzyme traces obtained on this nanomole scale, within minutes, and on the fly. The mini-ISES technique is applied here for the exploration of novel chiral space, with the goal of identifying fundamentally new scaffolds for asymmetric catalysis.

As one thinks about organizing chiral space for the design of asymmetric catalysts, the notion of symmetry often emerges. It has been argued, for example, that by building C_2-symmetry into a ligand or catalyst,

Department of Chemistry, University of Nebraska, Lincoln, NE 68588–0304, USA.
*Corresponding author. E-mail: dberkowitz1@unl.edu

one limits the number of chiral approaches available to substrate. In addition, although this can certainly be advantageous, as is illustrated in Fig. 1, "privileged chiral scaffolds" (*64*) for asymmetric catalysis are known that present chiral space in both C_2-symmetric (A) and non–C_2-symmetric senses (B). It is important to explore both topological domains in seeking to identify new chiral motifs of value (*65*). Among the chiral elements that have been invoked to carve out useful chiral space is axial chirality, from established ligands such as the BINAPs (Noyori) (*66*) to exploratory ligands being developed today around aniline systems with hindered rotation about C–N bonds (Curran) (*67*). Planar chirality is now an established chiral element, as highlighted by the success of the Phanephos (Pye) (*68*) and Josiphos ligands (Togni) (*69*), as well as related ferrocene-based scaffolds (*70*), including planar chiral "DMAP equivalents" (Fu) (*71*). Helical chirality is a chiral element still in its infancy for the chiral ligand design, with important recent contributions from Takenaka (*72*, *73*).

That said, catalysts projecting central chirality in a non–C_2-symmetric sense are of great importance in modern asymmetric synthesis, including those derived from chiral pool elements. These include proline-based oxazaborolidines (Itsuno, Corey) (*74*, *75*) and proline-containing β-turn–based systems (Miller) (*43*, *76*–*79*) in the domain of amino acids, not to mention proline itself, around which a plethora of organocatalytic transformations have been developed (*80*–*87*). The cinchona alkaloid–based systems are especially versatile, with proven efficacy in the asymmetric dihydroxylation of alkenes (Sharpless) (*88*), in asymmetric phase transfer alkylation (O'Donnell, Lygo, Corey) (*89*–*91*) and in asymmetric fluorination (Cahard) (*92*, *93*). On the C_2-symmetric side, tartrate esters (Sharpless) (*94*) and their derivative TADDOLates (Seebach) (*95*) also appear to be "privileged."

This notion of "privileged" scaffolds has its origins in medicinal chemistry, harking back to the 1988 paper from Evans and the Merck med chem group, in which the term was used to describe benzodiazepine-type

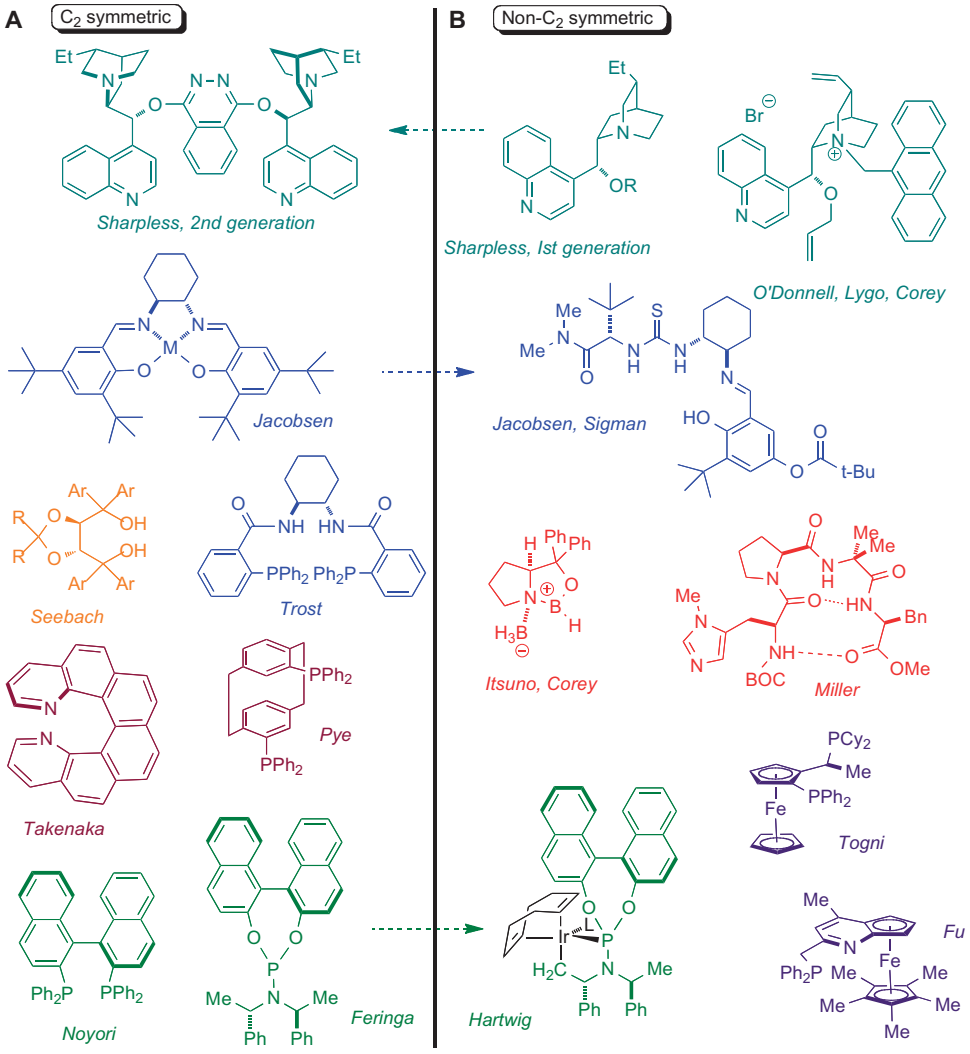

Fig. 1. "Privileged" chiral scaffolds. (**A**) C_2-symmetric scaffolds for asymmetric catalysis. Cinchona alkaloids (teal); *trans*-1,2-diaminocyclohexane systems (blue); TADDOLates (orange); Phanephos-planar chirality, helically chiral bipyridyl-type ligand (wine); BINAP systems (green). (**B**) Non–C_2-symmetric scaffolds. Cinchona alkaloids (teal); *trans*-1,2-diaminocyclohexane-based Strecker catalyst (blue); proline-based systems-oxazaborolidine (red); Phanephos-planar chirality, helically chiral bipyridyl ligand (wine); planar chiral ferrocenyl phosphine systems (purple); CH-activated Ir-phosphoramidite catalyst (green). Arrows indicate the conversion of C_2-symmetric systems into non–C_2-symmetric systems.

structures for neuroactive ligands (*96*). The concept persists in medicinal chemistry circles and has been discussed more recently by Stockwell (*97*). In such discussions, ligands are presumed to have a particular propensity to bind to a range of protein targets and influence function. "Privileged chiral ligands," on the other hand, it might be said, have a particular propensity to impart useful chiral bias to a catalytic center, usually upon ligation to a metal. This concept appears to have evolved from the medicinal chemistry concept and has been widely discussed in synthetic chemistry circles since the provocative piece in *Science* by Yoon and Jacobsen in 2003 (*64*).

Perhaps most interesting in this discussion of "privileged" chiral space and symmetry is the observation that depending on the system, advantage can be gained from both inducing C_2-symmetry where it is absent and breaking C_2-symmetry where it is present (see arrows depicting these "symmetry crossovers" in Fig. 1). Thus, Sharpless and co-workers generally improved upon the first-generation dihydroxylation ligands by constructing bidentate cinchona ligands into which a new C_2-axis is thereby built (*98*). On the other hand, while retaining the *trans*-1,2-diaminocyclohexane chiral scaffold from the "privileged" Jacobsen-type salens (*64*) and Trost-type bis-phosphines (*99*) , Jacobsen and Sigman later found it advantageous to place this same chiral scaffold into a non–C_2-symmetric system, presumably to generate a more enzyme-like system, with dual catalytic roles, in building an asymmetric Strecker catalyst (*40*). Perhaps most interesting in this category is the fortuitous finding by Hartwig and associates that "privileged" C_2-symmetric phosphoramidite ligands pioneered by Feringa (*100*–*102*), at least in the context of Ir-catalyzed allylic amination, lead to a very effective iridicyclic catalyst through a symmetry-breaking C–H activation event (*103*–*105*).

Our approach herein was to examine non–C_2-symmetric central chirality, and to investigate topologies not previously explored (*106*), with a particular focus on chiral 1,2-diamines and their derivative salens as chiral motifs with wide-ranging potential in asymmetric catalysis. Systems built around amino acid, terpenoid, and carbohydrate scaffolds were initially explored. A new set of interesting salen ligands built around the fructopyranosyl-4,5-acetonide emerged from these studies. We use mini-ISES to fingerprint the asymmetric profile of a focused array of ligands of this new class here. Key variables that have emerged include the ability to tune the shape of these ligands through the presence or absence of an anomeric effect and the ability to pair such non–C_2-symmetric 1,2-diamines with nonsterically demanding salicylaldehyde equivalents, to produce the most selective salen ligands yet observed, particularly in cases of "matched" substrates.

RESULTS

In the cassette ISES approach, multiple candidate catalytic combinations are screened in an information-rich parallel format. The experimentalist gleans data on relative rate, sense and magnitude of enantioselectivity, and substrate generality for the catalyst candidates being evaluated. The process is truly in situ, obviating the need to take aliquots or quench the reaction to obtain readouts on reaction progress. The hydrolytic kinetic resolution (HKR) serves as a very useful platform for both the investigation of new catalyst screening modalities and the development of new salen ligands, with the picture of a stereochemistry-determining transition state involving bimolecular metal-salen participation (vide infra) emerging (*107*–*110*).

Mini-ISES

The experimental configuration developed for mini-ISES is illustrated in Fig. 2 for the screening of Co(III)-salen catalysts for the HKR of epoxides, using both (±)-propylene oxide and (±)-hexene oxide as test substrates. The product 1,2-diols diffuse from the lower organic layer (20 μl) into an upper aqueous buffer layer (90 μl) containing reporting enzymes that oxidize the product, resulting in the conversion of NAD^+ (nicotinamide adenine dinucleotide) to NADH (reduced form of NAD^+) with a concomitant increase in the Abs_{340} observable by UV/vis spectroscopy. The experimental setup used herein uses 4 of 16 available 110-μl wells in a single quartz micromulticell per catalyst candidate and substrate pair, significantly streamlining the process. Additionally, as is described in detail below, three new KRED (ketoreductase; Codexis naming system) reporting enzymes have been identified, also serving to facilitate implementation of this information-rich, in situ screening methodology. Specifically, KRED 23 was found to be a complement to TBADH (*Thermoanaerobium brockii* alcohol dehydrogenase) for following the HKR of propylene oxide. The former is selective for (*S*)-1,2-propanediol and the latter for the (*R*)-antipode (see the Supplementary Materials for detailed kinetic analysis and data). For the HKR of hexene oxide, KRED 119 was identified as an (*R*)-selective reporting enzyme and KRED 107 as a highly (*S*)-selective enzyme.

After considerable experimentation with these reporting enzymes and the quartz micromulticell platform, it was found that the aqueous reporting layer could be reduced from 500 μl (cuvette-ISES) to 90 μl. The organic layer volume could be reduced from 300 to 20 μl in the micromulticell well, allowing for a significant reduction in the amount of catalyst/substrate needed for screening. Even under these mini-ISES conditions, reliable UV/vis spectroscopic traces were obtained from the reporting enzyme window. In terms of loading for mini-ISES, it was found that under optimal conditions, one can obtain useful ISES traces using only 200 to 350 nmol of active Co(III)-salen catalyst (0.25 mol %) within minutes (Fig. 2B). The salen ligand stereopreference profiles obtained are presented below, following a discussion of the design of this focused salen array and the synthesis of this new ligand class.

Design of the salen array

The original salen array that we assembled for double cuvette-ISES (*48*) was composed of 1,2-diamines derived from the chiral pool. Terpenoid, amino acid, and carbohydrate scaffolds were all fashioned into 1,2-diamines that were combined with variously substituted salicylaldehyde or α-hydroxy aryl aldehyde partners to generate the salen/pseudosalen array. Two particularly intriguing new salen motifs emerged from those early studies. On the one hand, a salen derived from the β-pinene–derived 1,2-diamine and α-hydroxynaphthaldehyde showed high *E* values for the HKR of matched terminal epoxides. This chiral diamine was new to asymmetric synthesis and was inspired by the success Midland (*111*) and Brown (*112*) had enjoyed in building chiral organoboron reagents from the α-pinenoid scaffold, most notably Alpine-borane and DIP-chloride. Indeed, this terpenoid β-pinene–derived pseudosalen ligand served as the source of all chirality in the rapid asymmetry assembly of the antipodal oxabicyclo[4.3.1]dodecyl cores of the sesquiterpene lactone natural products zaluzanin A and linearifolin in these laboratories (*45*).

D-Carbafructopyranose–based 1,2-diamines

The more provocative ISES lead was generated by exploring the fructopyranose scaffold as a new chiral scaffold around which to build

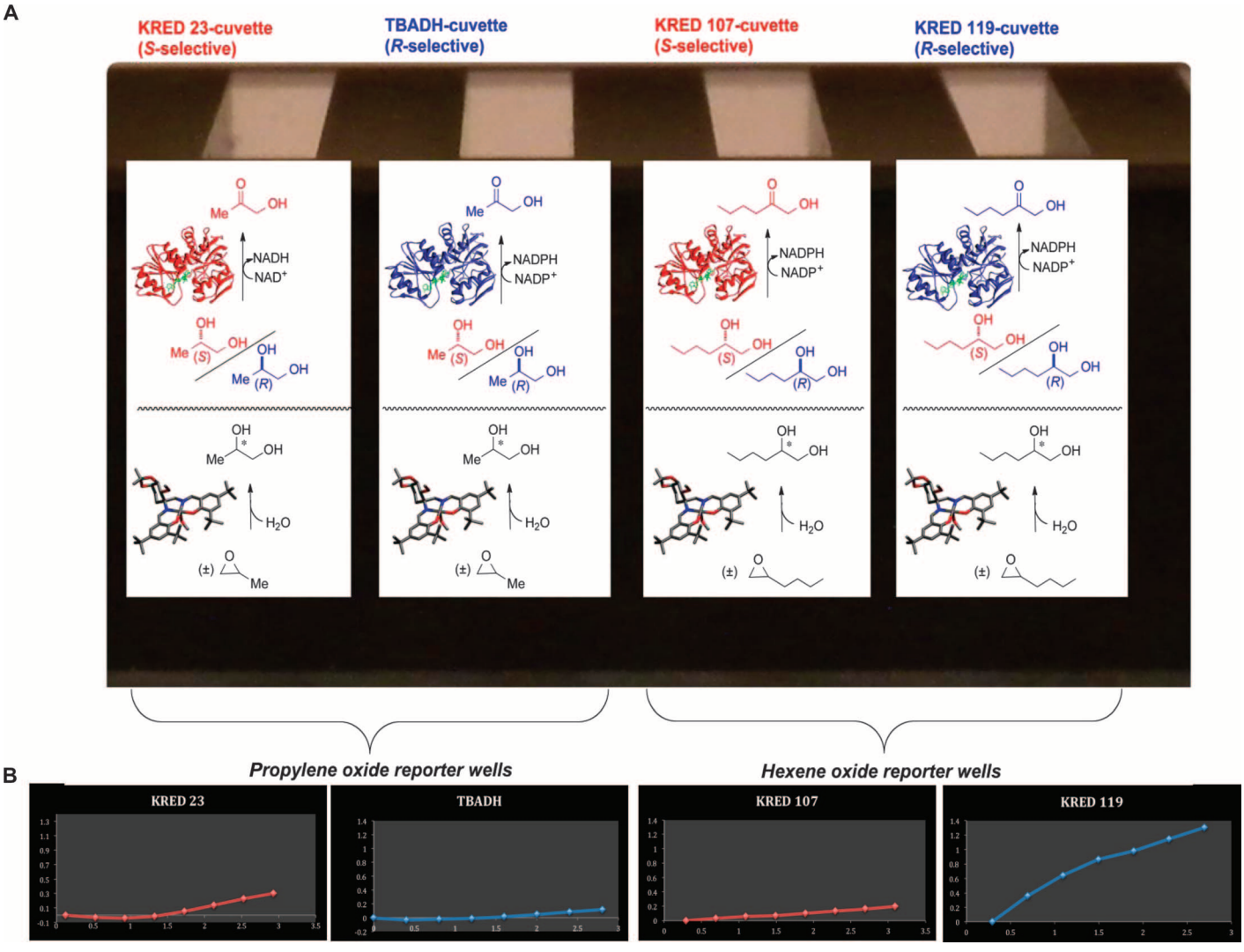

Fig. 2. Depiction of the mini-ISES format for information-rich catalyst screening (*ee*, relative rate, and substrate scope). (**A**) Quartz micromulticell in the background; reporting wells for catalyst derived from salen **16a** in the foreground featuring both (*S*)- and (*R*)-selective dehydrogenase reporting enzymes for both propylene oxide (KRED 23 and TBADH, respectively) and hexane oxide (KRED 107 and KRED 119, respectively). The protein structure shown is the actual structure of TBADH (PDB 1YKF). (**B**) Actual ISES data for the HKR of the respective epoxides mediated by the Co(III)-salen catalyst derived from **16a** in the lower organic layer (20 μl); spectral data reflect the conversion of $NAD(P)^+$ to NAD(P)H upon diol oxidation by the respective reporting enzyme, with the concomitant increase in $Abs_{340\ nm}$ versus *t* (min).

1,2-diamines. Prior to our work, D-fructose–based chirality had been used in both the furanose form (diphosphite ligands for Ni-mediated alkene hydrocyanation) (*113*) and the pyranose form in the seminal work of Shi (*114*, *115*), in which the 3-position of the sugar supports a chiral dioxirane moiety for alkene epoxidation. Against that backdrop, we chose to explore the D-fructopyranose-4,5-acetonide scaffold as a bicyclic chiral 1,2-diamine backbone. This appears to be the first example of the use of fructose-based chirality in 1,2-diamine ligand design. Figure 3 illustrates how the α- (*5*) and β-D-fructopyranosyl-1,2-diamines (*6*) can be readily assembled in six steps from D-fructose itself. Because of promise seen in the D-fructopyranose–based 1,2-diamines as new chiral motifs for asymmetric catalysis and the desire to prevent anomerization, it was decided to explore the corresponding carbocyclic system.

Our initial entry into the projected D-carbafructosyl-1,2-diamine scaffold emanates from (−)-quinic acid, as outlined in Fig. 4. The selective capture of the quinate carboxylic acid functionality as the 1,3-diaxially disposed lactone is based on the elegant work of Shing (*116*). This permits for the simultaneous blocking of the remaining vicinal diol via a cyclohexanone-derived ketal. Lactone cleavage then releases a single secondary alcohol allowing for site-selective oxidation. Pyridinium chlorochromate (PCC)–mediated oxidation then proceeds smoothly with concomitant elimination of the tertiary alcohol into the α,β-unsaturated ketone **8**. Sodium borohydride–mediated carbonyl reduction from the convex face followed by tranketalization leads to α,β-unsaturated ester **9**. Barton deoxygenation is followed by bis-Grignard addition into the methyl ester, giving triol **10**. The triol was selectively *O*-methylated at the lone secondary alcohol in the triol followed by

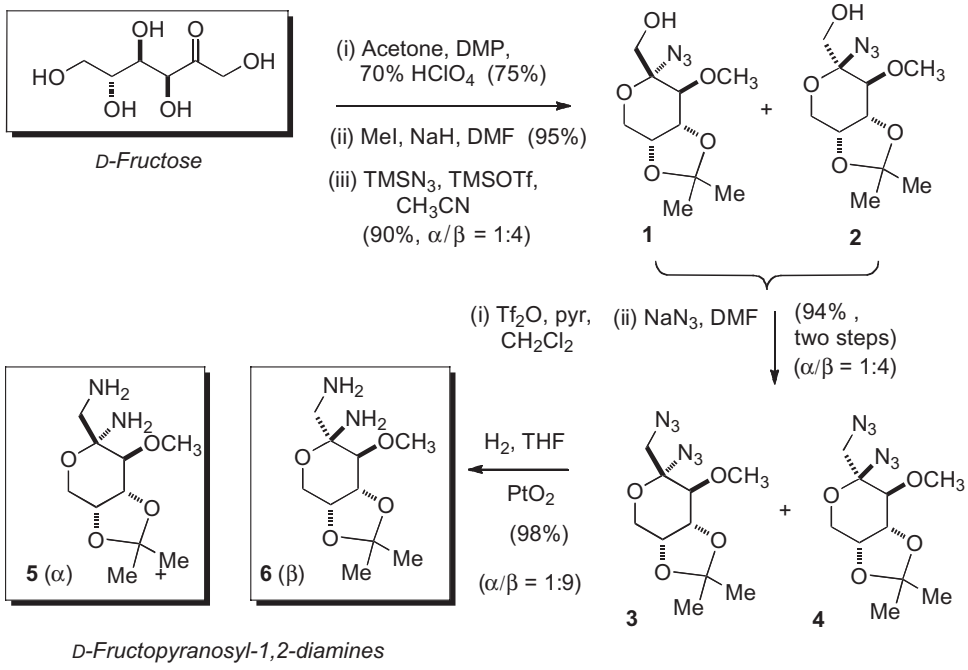

Fig. 3. D-Fructopyranosyl-1,2-diamine synthesis.

oxidative cleavage of the vic-*tert*-diol with $Pb(OAc)_4$ to yield stereodefined ketone **12**. Subsequent Wittig methylenation produced the desired carbofructose-leading olefin **13** in 80% yield. Next, the key step, diazidation of the exocyclic alkene, was realized, adopting a procedure developed by Snider and co-workers (*117*). Namely, $Mn(OAc)_3$-mediated alkene diazidation delivered the D-carbafructopyranosyl-1,2-diazide as a mixture of the anticipated α- (*14*) and β-pseudo-anomers (*15*). After chromatographic separation, these diastereomeric diazides were hydrogenated to give the respective diamines, **16** and **17**, as desired, in quantitative yield.

Assembly and screening of focused carbafructopyranose-based Co(III)-salen array

With both the oxa- and carbacyclic fructopyranosyl-1,2-diamines in hand, we next constructed a focused library of Co(III)-salen catalysts as depicted in Table 1. The α- and β-diastereomers of both the oxacyclic (*5*, *6*) and carbocyclic D-fructopyranosyl-1,2-diamines (*16*, *17*) were paired with salicylaldehydes bearing varied 3′,5′-substitution patterns [di- (**a**) or mono-*t*-butyl (**b**), diiodo (**c**)], as well as with the α-hydroxy-β-naphthaldehyde (**d**). Each salen was converted to the Co(II)-salen (precipitates out) by incubation with $Co(OAc)_2$ in MeOH. Immediately before performing HKR runs, the Co(II)-salen was converted to the Co(III)-salen(DNB) complex, by air oxidation in the presence of 3,5-dinitrobenzoic acid.

The newly developed mini-ISES was used for a rapid screening. As discussed, on the basis of diol oxidation efficiency and stereoselectivity, KRED 107 and KRED 119 were selected as reporting enzymes for the HKR of (±)-hexene oxide, whereas KRED 23 and TBADH were used to screen the HKR of (±)-propylene oxide. Then, by using a standard UV/vis apparatus, outfitted with the quartz micromulticell, the focused salen array could be expeditiously screened across both test substrates (see the Supplementary Materials for detailed characterization).

ISES-estimated *ee* values were compared with the measured *ee* values under typical flask conditions. Three-dimensional (3D) bar graph representations of these results are depicted in Fig. 5. The ISES screen involves biphasic organic ($CHCl_3$, epoxide)/aqueous conditions, wherein one sample diol product diffuses into the aqueous layer at early times and with minimal catalyst loading (0.25 mol %). On the other hand, the "flask conditions" here involve incubation of Co(III)-salen catalyst in neat epoxide, with 0.55 eq. water, at longer times (3 hours) and somewhat higher catalyst loading (0.5 to 1 mol %). The goal is to explore how well a rapid early screen serves to predict kinetic resolution efficiency.

As can be seen in the 3D bar graph patterns for ISES estimations of product *ee* at early times (Fig. 5, left side, blue/green bars) versus the high-performance liquid chromatography (HPLC) determinations of product diol *ee* under flask conditions (right side, pink, aqua bars), ISES serves as a useful, predictive screening tool here. In particular, one notes the clear (*S*)-selectivity of both Co(III)-**5c**-DNB and Co(III)-**17c**-DNB from the paired positively oriented bars, representing the two test substrates across both bar graphs. These catalysts, particularly those derived from the novel β-D-carbafructopyranosyl-1,2-diamine, **17c**, emerged from this focused screen as worthy of much greater study here. From a catalyst screening point of view, these initial studies demonstrate proof of principle for the ability to obtain reliable ISES data in this new micromulticell format, that is, mini-ISES. Recall that these data were obtained with the 20-μl organic layer/90-μl aqueous reporting layer volumes described and required nanomolar levels of catalyst per micromulticell well.

Structure/enantioselectivity relationships

In examining the patterns seen in this focused salen library screen, two interesting observations emerge, both unexpected and both useful in thinking about ligand structure/enantioselectivity relationships. First, in both the carbacyclic and oxacyclic series, an "enantioswitch" is

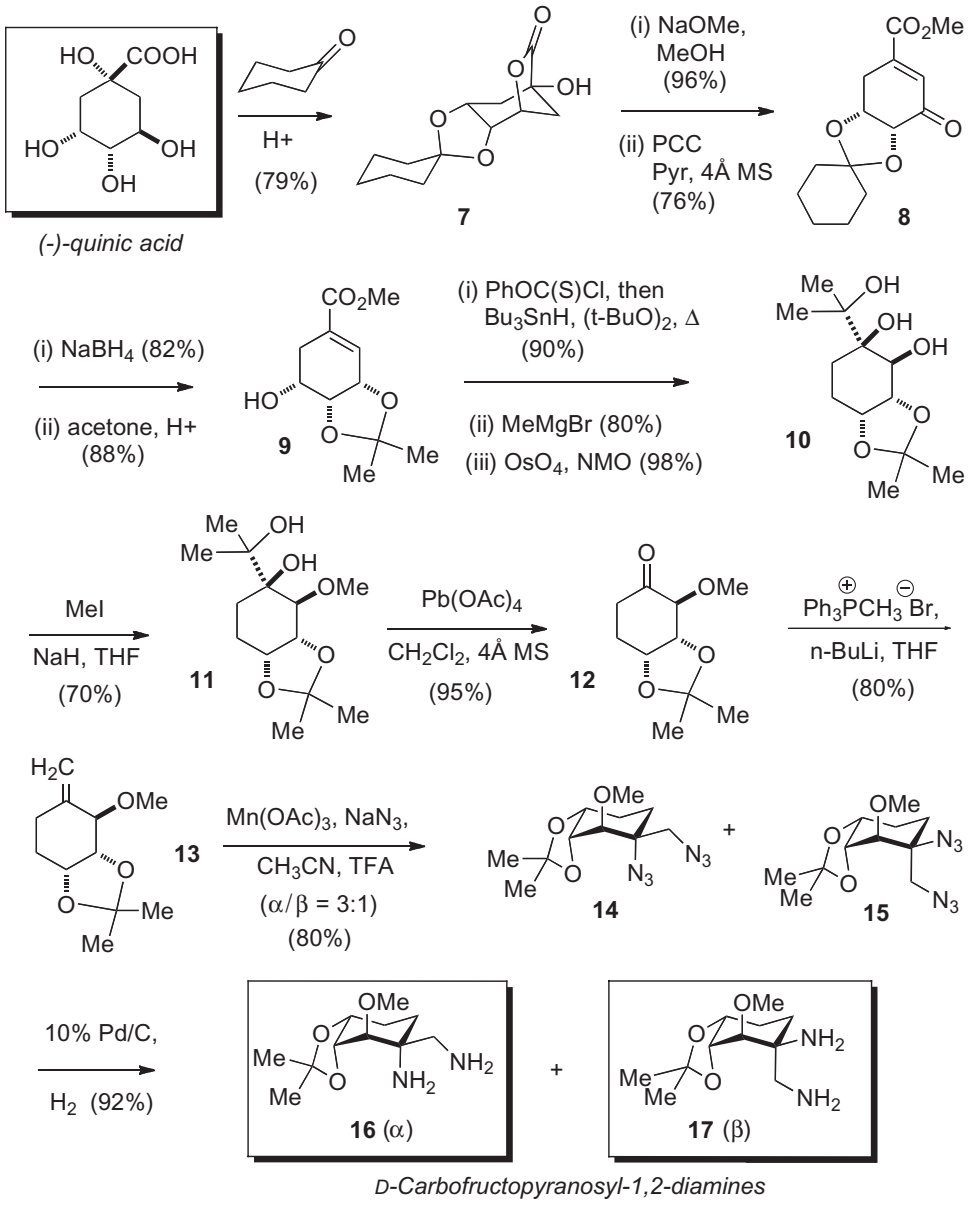

Fig. 4. Synthesis of α- and β-D-carbafructopyranosyl-1,2-diamines from quinic acid.

observed based on the substituent on the salicylaldehyde and not the chiral element, that is, the D-fructopyranose–based 1,2-diamine. Specifically, when evaluated for the HKR of propylene oxide and hexene oxide, the Co(III)-salen catalyst derived from the pairing of the β-D-carbafructopyranose-1,2-diamine (*17*) with 3,5-di-*tert*-butylsalicylaldehyde (**a**) gives rise to the (*R*)-diol products, whereas the catalyst derived from pairing of this same chiral diamine (*17*) with 3,5-diiodosalicylaldehyde (**c**) gives the corresponding (*S*)-diol products. This is the same pattern that is seen in the oxacylic (native fructose-derived) series with the true β-D-fructopyranosyl-1,2-diamine (that is, **6a** versus **6c**). However, given that **6** and the corresponding α-anomer **5** can interconvert via an anomerization mechanism, one could always hypothesize that in the oxacyclic series, an undetected anomerization might somehow underlie this apparent "enantioswitch" in catalyst preference. The result with the carbacyclic system (that is, **17a** versus **17c**) now seems to firmly rule out this "undetected anomerization" mechanism for change of enantiopreference in the oxa-fructopyranose series. The overall result here is important. Namely, within the context of these new carba- and oxacyclic β-D-fructopyranosyl-1,2-diamine chiral scaffolds, one can alter the sense of enantiopreference and improve the magnitude of enantioselection by moving from the more sterically encumbering 3′,5′-di-*tert*-butyl substitution pattern on the salen to the less sterically encumbering 3′,5′-diiodo substitution pattern.

However, probably the most interesting and informative observation made here is the notable enantioselectivity improvement from the oxafructopyranose-based ligand **6c** to the carbafructopyranose-based

Table 1. HKR screening of focused oxa/carbafructopyranose-derived salen array. Each box provides the HKR data of propylene oxide (black) and hexene oxide (blue) under the catalysis of the corresponding Co(III)-salen 3,5-dinitrobenzoate. The ISES-estimated % *ee* values of the produced diols are presented in brackets, followed by the observed % *ee* values (chiral HPLC) and calculated *E* values.

	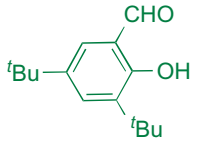 a	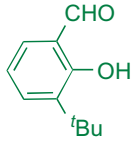 b	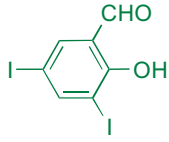 c	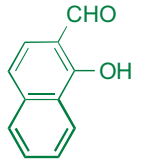 d
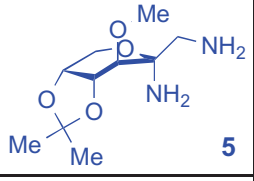 **5**	[77(+)] 69(+) *6.2(+)* [64(+)] 45(+) *4.0(+)*	[70(+)] 42(+) *2.6(+)* [67(+)] 40(+) *2.4(+)*	¶	§ # 25(+) *1.7(+)*
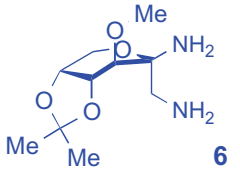 **6**	[33(−)] 64(−) *4.7(−)* # 52(−) *4.2(−)*	[28(−)] 40(−) *2.5(−)* [31(−)] 36(−) *2.4(−)*	[85(+)] 83(+) *13(+)* [77(+)] 85(+) *28(+)*	§ §
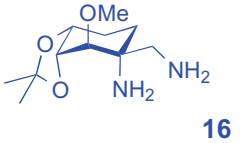 **16**	[53(−)] 37(−) *2.3(−)* [23(−)] 29(−) *2.0(−)*	[76(−)] 75(−) *8.2(−)* [40(−)] 45(−) *3.5(−)*	[91(−)] 85(−) *17(−)* [42(−)] 63(−) *5.0(−)*	[78(−)] 61(−) *4.3(−)* [59(−)] 55(−) *3.8(−)*
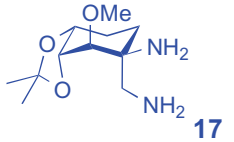 **17**	[39(−)] 28(−) *1.9(−)* # 30(-) *2.1(-)*	[67(−)] 48(−) *3.4(−)* [50(−)] 53(−) *3.4(−)*	[94(+)] 93(+) *44(+)* [77(+)] 92(+) *104(+)*	§ [13(−)] 34(−) *2.2(−)*

¶Difficulty was encountered in synthesizing appreciable quantities of this salen. #These catalysts gave negligible ISES rates. §These catalysts gave a conversion < 2% after 72 hours.

ligand **17c**. Replacing the ring oxygen with a methylene confers a significantly higher (*S*)-selectivity upon the resulting Co(III)-salen complex, with an about three- to fourfold increase in *E* value—from 13 to 44 and from 28 to 104 for the HKR of the propylene and hexene oxides, respectively. This experimental observation prompted us to examine the underlying structural basis of such a dramatic change in chiral bias by single atom replacement. Of course, it had not escaped our attention that this particular single-atom replacement could have important structural consequences, as one would be effectively removing a ground state anomeric effect, such as it is, in such a diamino-sugar system. For these reasons, complete crystallographic characterization of these Co-salens was undertaken and provides important insight in this regard, as is discussed in detail below.

Benchmarking performance for the carbofructopyranosyl-1,2-diamine–derived salen-17c

To assess the potential of the most promising ISES hit for asymmetric catalysis, the top mini-ISES hit, catalyst Co(III)-(**17c**)-DNB, was next taken well beyond the screening set and examined for its HKR performance across a range of differentially structured and substituted epoxide substrates. The results are collected in Table 2. Given the difficulty in obtaining accurate values for the selectivity factor for any kinetic resolution, we find it useful to measure yield and *ee* of both the remaining epoxide and the product diol, in each case. This provides two independent measures of enantioselectivity for each entry and, we feel, lends more confidence in assigning these values as a measure of catalyst performance with a particular substrate. The results are rather striking. The Co(III)-**17c**-DNB catalyst exhibits excellent HKR results with three substrates, displaying *E* values in the range of 40 to 50, whereas nearly perfect resolutions are obtained for another three substrates, namely, hexane oxide, *O*-phenylglycidol, and 3-phenylpropylene oxide.

For benchmarking purposes, the latter two epoxides are of particular interest, because they have been the targets of both asymmetric metal-salen–based and biocatalytic efforts directed at developing new and efficient HKR catalysts. (1a) For *O*-phenylglycidol, *trans*-1,2-diaminocyclohexane–based Co(III)-salens have been used by both the Schulz (*118*) and Jacobsen groups, with reported *E* values ranging from 60 (54% conversion) to 120 (18% conversion), respectively.

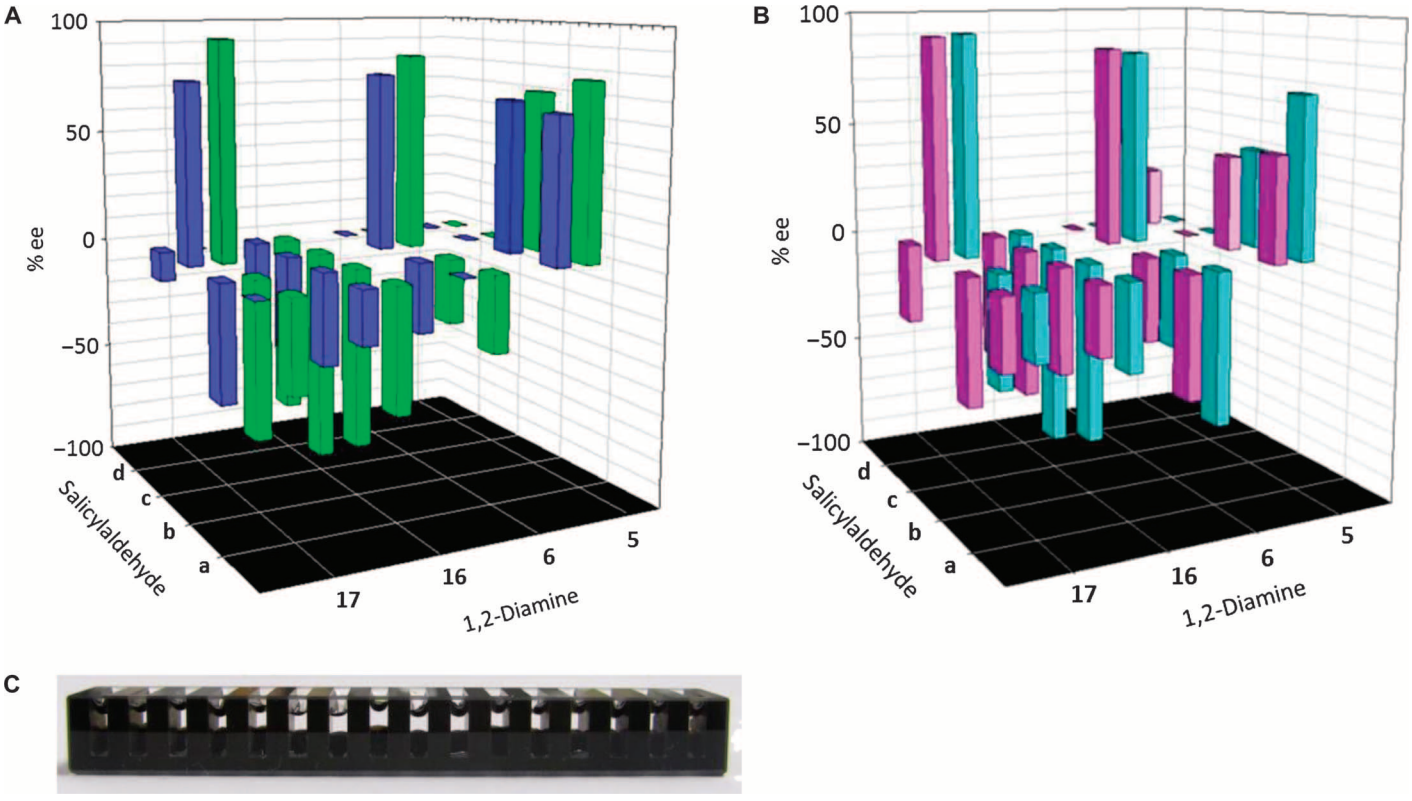

Fig. 5. Three-dimensional bar graph for data from miniaturized ISES-for the Co-salen array. (**A**) ISES data displayed in 3D format. (**B**) Comparison data from flask reactions (see the Supplementary Materials for details). (**C**) Sixteen-well quartz micromulticell used for mini-ISES. Note: Positive deflection = *S*-selective; blue, pink = HKR of hexane oxide; green, aqua = HKR of propylene oxide.

(1b) On the enzymatic side, Reetz and co-workers have carried out two separate directed evolution studies, both emanating from native *Aspergillus niger* epoxide hydrolase (ANEH) and both directed at developing enzymatic catalysts optimized for the HKR of *O*-phenylglycidol. In the first case, 20,000 clones were generated in a five-step process resulting in an evolved ANEH with nine point mutations and an *E* value of 115 (*119*). A more recent study, in which ePCR was first used, expression levels led to a new ANEH variant with seven point mutations, plus a 13-mer peptide insertion (apparently an unintended consequence of the QuikChange protocol for site-directed mutagenesis) (*120*). This new directed evolution mutant shows an *E* value of 160 for the HKR of *O*-phenylglycidol. Thus, Co(III)-**17c** shows a chiral bias ($E = 95 \pm 2$ at 51% conversion) comparable to the best-known chiral Co-salen catalyst ($E = 90 \pm 30$ at 18 to 54% conversion) but somewhat lower than the best-evolved enzymes for this reaction ($E = 115$; 160). For the HKR of 3-phenylpropylene oxide, (2a) the *trans*-1,2-diaminocyclohexane–based Co(III)-salen due to Jacobsen is the most selective metal-organic catalyst previously reported, with $E = 96$ (20% conversion) (*110*). (2b) In the enzymatic realm, in this case, the Widersten group recently described the directed evolution of a plant enzyme, *Solanum tuberosum* epoxide hydrolase (StEH), targeted at the HKR of this substrate. Through four cycles of directed evolution, the best variant featured five point mutations and displayed $E = 14$ (*121*). Then, the Co(III)-**17c** catalyst introduced here shows a chiral bias ($E = 106 \pm 13$ at 51% conversion) that is at least equivalent to the best-known chiral salen catalyst ($E = 96$ at 20% conversion) and superior to the best enzymatic catalyst ($E = 14$) yet described.

X-ray crystallographic analysis: Tuning ligand shape via the anomeric effect

To gain further insight into the chiral space mapped out by these new chiral ligands and into the structural basis of the enantiopreferences displayed by the most promising catalyst, we next set out to obtain diffractible crystals. We report here the x-ray crystal structures of three Co(II)-salen complexes, namely, those derived from salens **6a**, **6c**, and **17c**. The 3D structures of each of these three new D-fructopyranose–derived salen scaffolds are displayed in Fig. 6. One sees very clearly that whereas both oxacycles assume a distorted $^{3,6}B$ boat-like structure for the pyranose ring, the carbacycle displays a $^{5}C_{2}$ chair-like geometry. The information gleaned here suggests that the shape of these ligands can be "tuned" by the anomeric effect (*122*). Thus, in the absence of an anomeric effect, in the carbacycle, the sterics of the Co(salen) system are apparently such as to favor a $^{5}C_{2}$ conformation for the cyclohexyl ring as is revealed by the structure of Co(II)-**17c** (Fig. 6C). Introduction of the ring oxygen into this system would produce the $^{5}C_{2}$ conformation depicted in Fig. 6A for the Co(II)-**6c** complex. As can be seen, this would introduce an unfavorable reinforcing dipole-dipole interaction between the anomeric C–N bond and the ring dipole (*123*). Distortion of the amino sugar core from a $^{5}C_{2}$ conformation to a $^{3,6}B$ conformer (Fig. 6B) serves to relieve this dipolar strain, thereby changing the shape

Table 2. Overview of HKR performance of the Co(III)-dinitrobenzoate catalyst derived from salen 17c. rt, room temperature.

Entry	Epoxide educt (±)	Catalyst loading (mol%)	Conditions[a]	Conversion[b]	Isolated epoxide[c]	Isolated diol
1	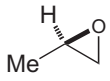	0.14	Neat, 0°C, 15 hours	45	50, −74, 44	46, 88, 34
2	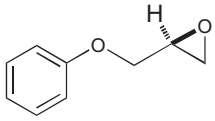	0.5	DCM, rt, 20 hours	51	47, −96, 97	46, 92, 93
3	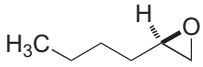	0.5	Neat, 0°C, 30 hours	52	45, −99, 104	48, 91, 116
4	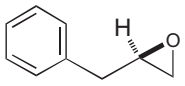	0.5	Neat, 0°C, 23 hours	51	48, −97, 119	49, 92, 93
5	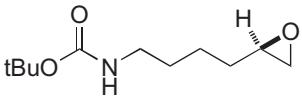	1.0	THF, rt, 35 hours	44	55, −72, 49	40, 92, 52
6	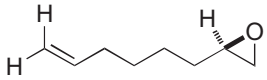	0.5	Neat, rt, 30 hours	54	40, −99, 61	48, 82, 40
7	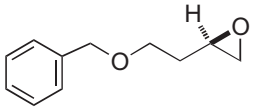	0.5	DCM, rt, 20 hours	32	68, −39, 16	26, 86, 20
8	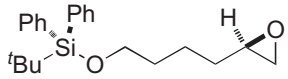	1.0	THF, rt, 50 hours	28	63, −33, 17	28, 90, 27

[a]Catalyst (0.2 to 1 mol %) was added to a solution of epoxide in THF or DCM or neat condition. The mixture was cooled to 0°C or kept at room temperature and 0.5 equivalent water was added to initiate the reaction. The reaction was stirred at 0°C or room temperature until completion. [b]Conversion of the reaction was determined by ^{1}H NMR. [c]The purified yield (black), % *ee* (red), and calculated *E* value (blue) are listed consecutively. Note: All diol products are presumed to be (*S*)-configured but, for entry 2, due to a change in Cahn-Ingold-Prelog prioritization. A negative sign as prefix for the % *ee* designates that the epoxide is (*S*)-configured.

of the ligand, the chiral space that it maps out, and the chiral bias that it manifests in the HKR reaction.

There is good precedent for the anomeric effect playing an important role in the pyranose forms of the parent sugars for all four of the diastereomeric ketohexoses. Thus, both β-D-fructopyranose (*124*) and β-D-psicopyranose (*125*) are known to assume the $^2C_5$ chair, whereas both α-D-tagatose (*126*) and α-L-sorbose (*127*) exist predominantly in the $^5C_2$ chair as pyranoses. In all such cases, the anomeric C–O bond is oriented so as to partially oppose the ring dipole. The amino sugar salens being investigated here differ from the parent sugar pyranoses, both in having an unusual anomeric C–N bond and in having both the C1- and the C2-nitrogens engaged in a rigid Co-salen ring system. We believe that this has the effect of distorting the normally favored chair conformer into a boat-like conformer that nonetheless displays a favorable anomeric effect (partially opposing dipoles) as is seen the structures for both Co(II)-**6c** and Co(II)-**6a** (Fig. 7, B and D, respectively). The removal of the ring oxygen in these systems not only locks out anomerization but also reshapes the ligand, by removing this boat-enforcing anomeric effect, generating an even more enantiodiscriminating chiral scaffold.

Considering bimolecularity in the HKR transition state

In seeking to model the favorable chiral bias (Table 2) exhibited by the Co(III)-**17c**-salen catalyst, we began from the crystal structure coordinates of the corresponding Co(II)-**17c** complex. Modeling was guided by three key observations from the Co(III)-salen HKR literature. (i) First, careful kinetic studies by Blackmond and Jacobsen indicate that two molecules of Co(III)-salen are involved in the HKR mechanism (*109*), one to deliver the hydroxide nucleophile to the epoxide and the other [likely bearing a DNB counterion (*108*); a second molecule of Co(III)-salen–OH is used here for the model] as a Lewis acid. Density functional theory (DFT) studies agree with these experimental observations, finding that a cooperative, bimolecular S_N2-like pathway for Co-salen–mediated epoxide hydrolysis is favored over unimolecular alternatives (*128*). (ii) The Chin crystal of an aziridine Co(III)-salen complex was used to guide both the coordination distance and

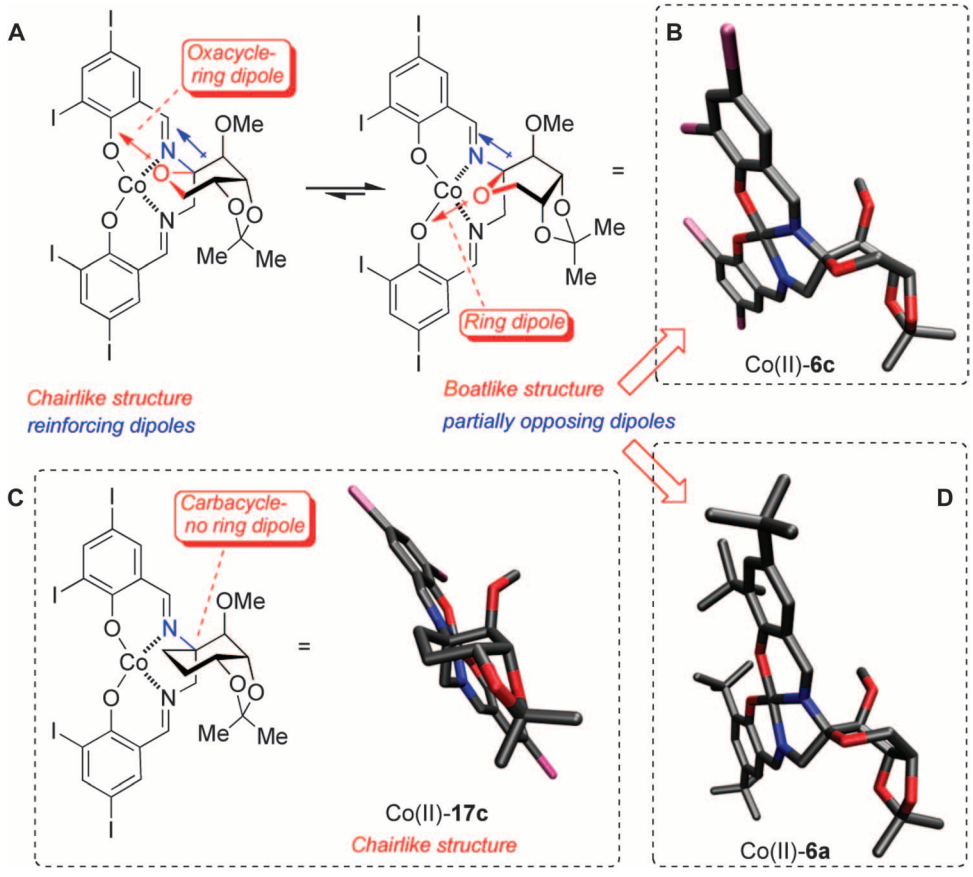

Fig. 6. X-ray crystal structures of Co-salen complexes reveal a correlation between anomeric effect and ligand shape in this ligand family. (**A**) Schematic drawing of the proposed distortion of a $^{5}C_{2}$-like conformation into a $^{3,6}B$-like conformation to minimize dipole-dipole repulsion in Co(II)-**6c**, as a manifestation of the anomeric effect. (**B** to **D**) X-ray crystal structures of (B) Co(II)-**6c,** (C) Co(II)-**17c**, and (D) Co(II)-**6a**.

coordination angle of the Co-salen–bound epoxide (*129*). (iii) A recent DFT computational study by Jacobsen and co-workers posits that key stereoelectronic control elements are at play in such Co-salen–mediated epoxide openings. Their studies project that the O–Co–O–C dihedral angle (θ) is critical, with the energy well for productive coordination complexes displaying a shallow minimum, suggesting that dihedral angles approximately in the 20 to 60° range are optimal (*107*).

As noted above, x-ray crystallography reveals a chair-like carbasugar ring in the Co(II)-**17c** structure. The Co(III)-**17c**-OH complex was built from these crystallographic coordinates, followed by docking of a typical terminal epoxide substrate, taking care to minimize unfavorable van der Waals interactions in so doing. The model obtained is presented in Fig. 8. (*S*)-hexene oxide is coordinated to the Co(III) center at 1.99 Å, close to the Co–N distance in the Chin crystal structure (1.95 Å). In addition, the oxirane ring approaches the Co center at an angle (122 ± 18°) modeled after that of the bound aziridine (123 ± 3°) in this structure. The dihedral angle is 24°, close to the O–Co–N–C angle observed in the Chin structure (33°) within the domain of the shallow minimum identified by the Jacobsen group. Adhering to these constraints, the (*S*)-hexene oxide substrate is well positioned underneath the π face of HO-Co-salen moiety, a face that is particularly accommodating with diiodo substitution. Finally, Jacobsen also puts forth the notion that enantioselection in such biomolecular salen-epoxide complexes may be governed by the overall stepped conformation of the Co-salen complex (*107*). To investigate this in the context of the new Co-salen complexes described here, the step heights for each of the three Co-salen crystal structures were estimated (see the Supplementary Materials for details) with the observation that the Co(II)-**17c** complex also displays the largest step height of the set at 0.76 Å. That the fructopyranose-based Co-salen complexes being investigated here by both crystallography and chiral bias display a similar structure/enantioselectivity relationship to that seen by Jacobsen and co-workers lends support to the notion that these systems proceed through similar mechanisms (for example, as modeled in the bimolecular transition state envisioned in Fig. 7).

Streamlined synthesis of β-D-carbafructopyranosyl-1,2-diamine

Given the promise shown by this previously undescribed β-D-carbafructapyanosyl-1,2-diamine chiral scaffold, we have now also developed a streamlined, second-generation entry into this system beginning from a cheap, readily available starting material, α-methyl-D-mannopyranoside (Fig. 8). Thus, an Appel reaction efficiently transforms the 6-hydroxyl into the 6-iodide. The requisite acetonide may then be selectively installed across the cis-configured vicinal 2,3-diol through exposure to dimethoxypropane/acetone with catalytic *p*-TsOH. C-4-*O*-methylation and dehydrohalogenation can then be achieved in a single step, in nearly quantitative yield, giving enol ether **19**. For the key type II Ferrier rearrangement, several divalent, late-transition metal catalysts [$HgCl_2$, $Pd(OAc)_2$, and $PdCl_2$] were examined, with

variation of solvent and temperature. The optimal conditions identified use 10 mol % $Pd(OAc)_2$ in a mixture of acetone, dioxane, and water (40:40:20) at 0°C, providing rearranged product **20** in 85% yield. The temperature proved to be critical, with warming the reaction to room temperature resulting in unwanted side products. To remove the resultant hydroxyl group in **20**, Barton deoxygenation was initially envisioned. However, the projected phenyl thionocarbonate ester proved to be unstable and tended to be eliminated upon exposure to silica gel. This observation led us to modify the route, adding an *O*-mesylation step to facilitate in situ β elimination to the α,β-unsaturated ketone intermediate in 80% yield. Hydrogenation then gives **12**, the key intermediate in the synthesis of **17c**, in quantitative yield. The newly developed synthesis saves six steps, raises the overall yield more than fivefold compared to the first-generation route from (–)-quinic acid, and also begins from a more economical starting material, namely, D-mannopyranose.

DISCUSSION

Inspired by recent developments in leading process chemistry groups to reduce the scale for reaction development and catalyst optimization down to the nanomolar regime (*61*), we report here a mini-ISES screen that exploits a quartz micromulticell for parallel screening of catalysts in 20-μl organic volumes at 200 to 350 nmol of catalyst loading. The technique is used to probe for diamine ligands and their derivative salens that map out new and potential useful chiral space for asymmetric catalysis. Out of these efforts emerged a new chiral motif built around the non–C_2-symmetric β-D-fructopyranosyl-1,2-diamine and its cognate carbacycle, particularly when combined when the sterically unencumbered 3′,5′-diiodosalicylaldehyde, to build salen ligands with promise for asymmetric catalysis. In pairing a non–C_2-symmetric diamine with a sterically unencumbered salicylaldehyde partner, this approach parts from conventional wisdom in metal-salen catalyst design and yet the swath of chiral space that results is clearly of value (see Fig. 9 for a schematic representation of the catalyst discovery and analysis pathway taken in this study).

From the point of view of chiral ligand development, there are two principal concepts that emerged from these studies. On the one hand, the β-D-carbafructopyranosyl-1,2-diamine scaffold is a potentially 'privileged' scaffold for the construction of chiral reagents and catalysts (*64*), although any such designation certainly must await much more extensive characterization of this new chiral framework across a greater breadth of salen-asymmetric and non–salen-asymmetric synthesis space. Thus, to our knowledge, the carbacyclic diamine, when incorporated into the Co(III)-**17c** catalyst, displays a chiral bias for the HKR of 3-phenylpropylene oxide (E = 106 ± 13 at 51% conversion) comparable to or better than that of the best catalysts reported heretofore, including the best such metal-salen catalyst (E = 96 at 20% conversion) (*110*) and the best such evolved enzyme (E =14) (*121*). For the HKR of *O*-phenylglycidol, this metal-salen appears to be equivalent (E = 95 ± 2 at 51% conversion) to the best known such catalyst (E = 90 ± 30 at 18 to 54% conversion) (*118*), and both of these metal-salens fall just short of the best-evolved enzymes (E = 115; 160) (*107*, *119*, *120*). These experimental observations attest to the potential of this new chiral scaffold for asymmetric catalysis.

The second interesting conceptual finding here relates to the tunability of these ligands, beyond the stereochemistry, substituent distribution, and bicyclic nature of the ring system in this non–C_2-symmetric chiral-1,2-diamine, and beyond its matched or mismatched pairing with

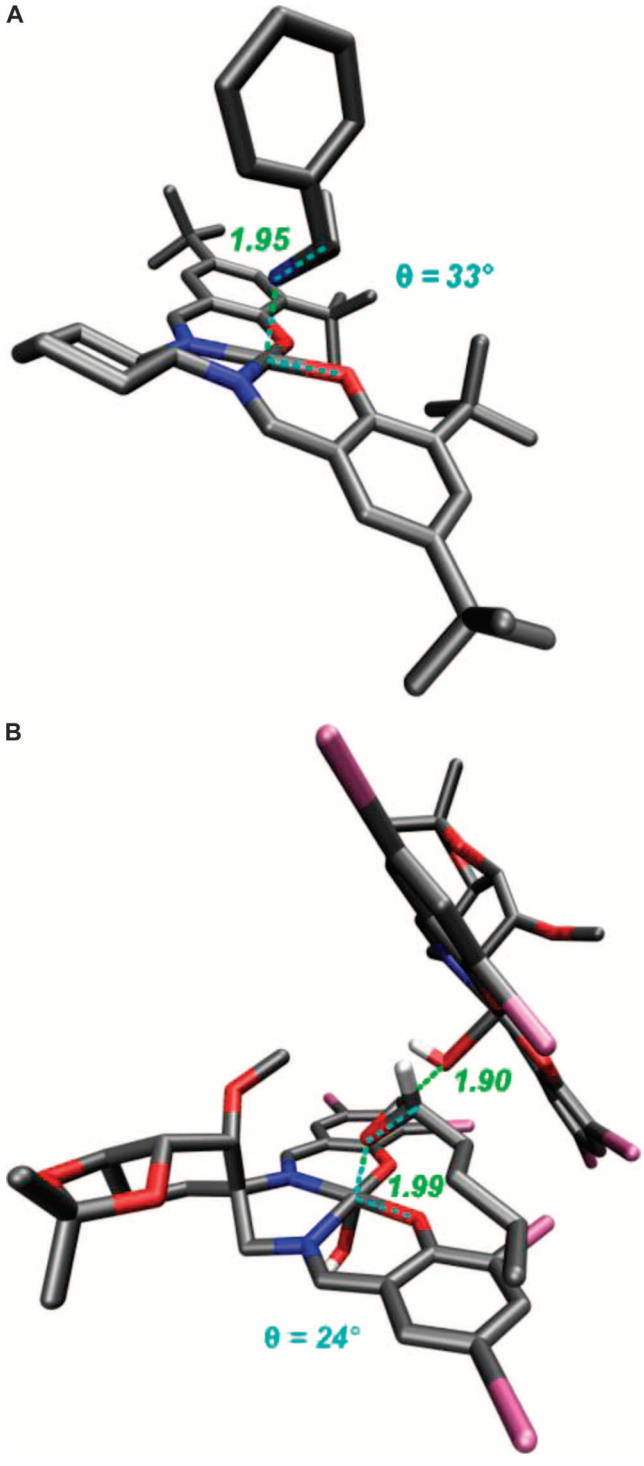

Fig. 7. Chin structure versus transition-state model for the HKR of hexene oxide with catalyst Co(III)-17c. (**A**) Chin's Co(III)-salen-aziridine complex (second aziridine ligand omitted for clarity). (**B**) TS model for the HKR of hexane oxide with catalyst Co(III)-**17c**. Note: The catalyst structure was built from the x-ray coordinates of the Co(II)-**17c** structure (Fig. 6C) using the Chin structure as a guide in Spartan. The preferred substrate enantiomer, (*S*)-hexene oxide, was docked (Accelrys) at a Co–O coordination bond length of 1.99 Å, similar to the Co–N distance in the Chin structure. The O–Co–O–C dihedral angle θ in the TS model is at 24°, within the preferred range described by Jacobsen and co-workers.

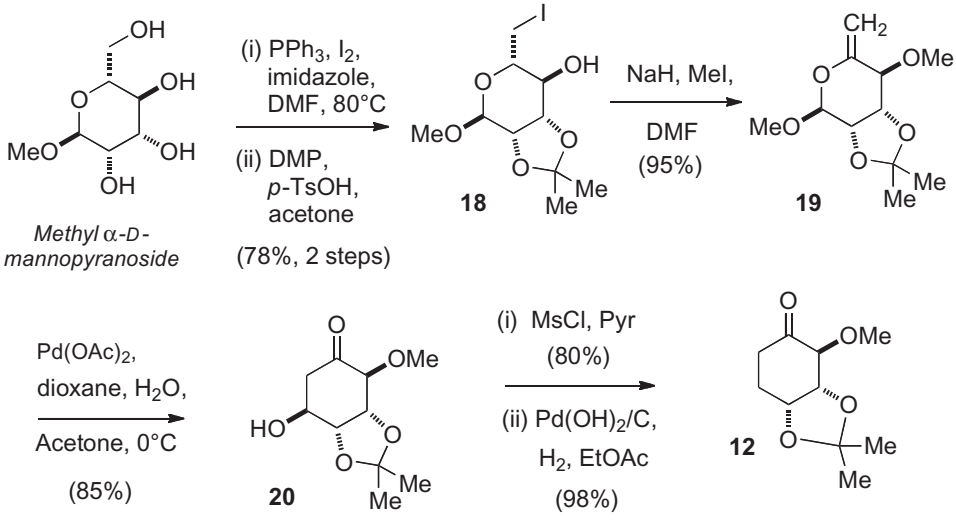

Fig. 8. Streamlined access into the key intermediate toward the β-carbafructopyranosyl-1,2-diamines from D-mannose.

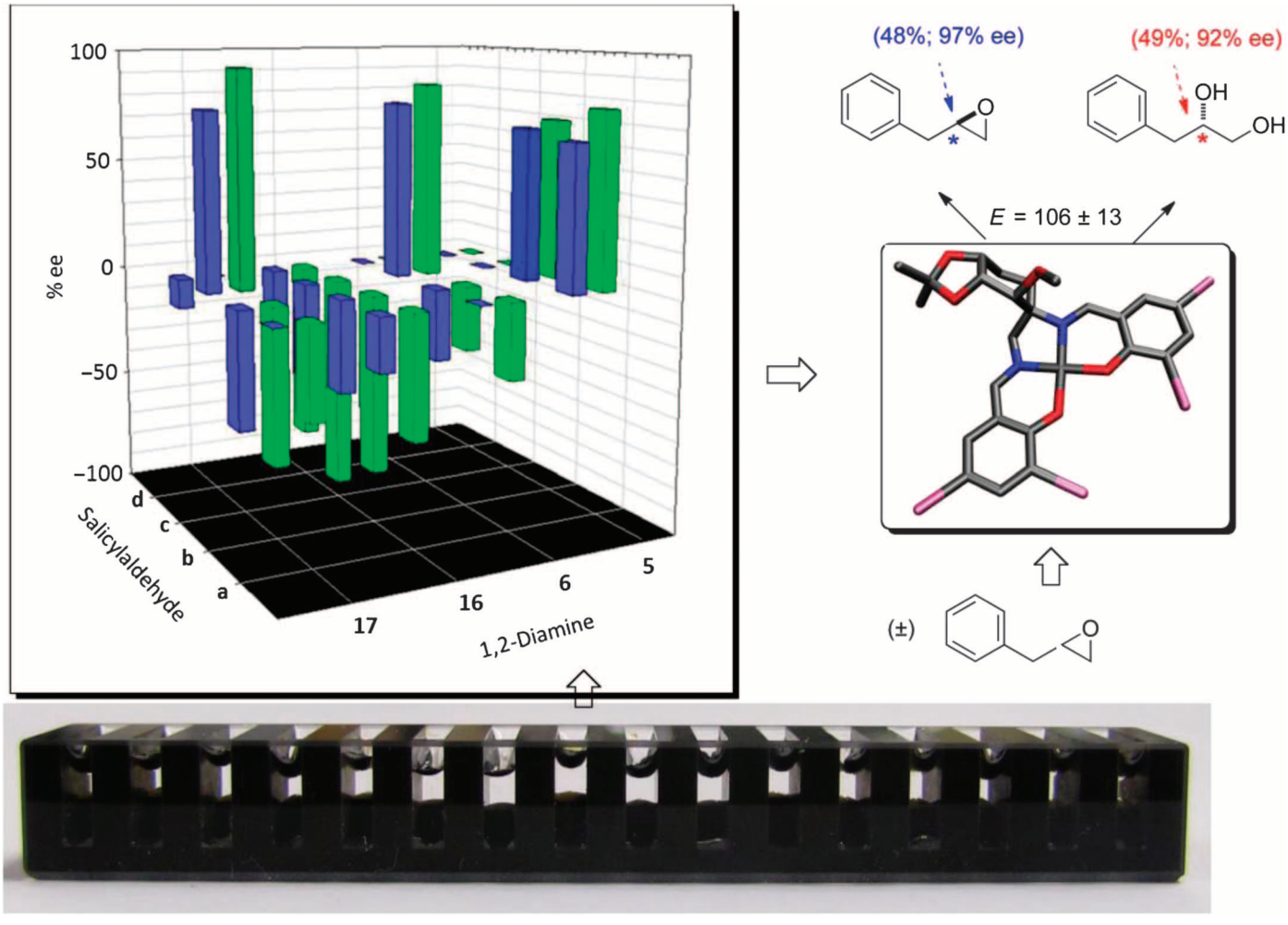

Fig. 9. Overview of the application of mini-ISES to the screening and identification of new chiral scaffolds for asymmetric catalysis. A focused salen array is screening in parallel by UV/vis spectrophotometry using a micromulticell (20-μl organic layer) so as to bring catalyst loading down to the nanomolar level. Reporting enzyme output can then be processed to give an in situ readout on sense and magnitude of enantioselectivity. Out of this study, the cobalt-**17c** salen complex emerged as a particularly promising catalyst, indeed the best catalyst reported to date for the HKR of 3-phenyl propylene oxide.

substituted salicylaldehydes. There is an important additional control element built into this diamine ligand scaffold, namely, the ability to modulate ligand shape significantly by introducing or removing an anomeric effect. Operationally, this amounts to a single heteroatom change, and to illustrate the underlying principle here, it is probably of advantage to run the thought experiment in the reverse direction to the actual experiment here. Thus, crystallographic studies demonstrate that the carbocyclic diamino-salen, Co(II)-**17c**, adopts a $^5C_2$ chair-like structure at its core (Fig. 6C). This confers a shape and overall step height that is commensurate with a highly enantioselective catalyst, at least for the HKR chemistry explored here. However, introduction of the sugar ring oxygen into Co(II)-**17c** would generate Co(II)-**6c** in a $^5C_2$ conformation that suffers from a significant ring dipole-anomeric C–N dipole reinforcement interaction, that is, an unfavorable anomeric effect (Fig. 6A). Distortion of the amino sugar core from a $^5C_2$ conformation to a $^{3,6}B$ conformation would relieve this dipolar strain, thereby changing the shape of ligand from chair- to boat-like at its core. This, in turn, fundamentally alters the chiral space that the ligand maps out, and the step height of the Co-salen complex, ultimately resulting in a changed chiral bias in the HKR reaction. We believe that this third degree of modularity of these ligands, grounded in the anomeric effect, adds an important dimension to their versatility as building blocks for the construction of salen ligands, as well as other chiral catalyst or reagent frameworks. In the future, other subtle modifications, such as fluorination, that could have large effects on dipole-dipole interactions (*123*) may be strategically employable to modulate such anomeric effect tuning approaches.

From a much broader catalyst evolution perspective, that substitution of a CH_2 for the ring oxygen boosts catalyst selectivity to the same approximate levels as two different highly evolved (directed evolution) epoxide hydrolase enzymes (*119*, *121*) attests to the validity of this approach to chiral ligand/catalyst discovery. It is worth noting here that whereas this type of "isostere" replacement approach is common in medicinal chemistry, it is much less common in other fields, although elegant and revealing examples in both chemical biology (for example, replacement of a native protein β turn with a synthetic prosthetic) (*130*, *131*) and in asymmetric catalyst design (for example, replacement of key amide bond with an alkene isostere) (*132*, *133*) have appeared in recent years. As for the notion that this "tunable" carbafructopyranosyl-1,2-diamine–derived ligand scaffold is "privileged," this will best be assessed through its further exploration across other metal-salen or chiral 1,2-diamine–mediated transformations both in these laboratories and beyond.

The ability to miniaturize the ISES method, using an uncomplicated commercially available micromulticell, should make this method accessible to broader application in chiral catalyst development and continue to move this methodology further into the nanomolar regime, in keeping with the trend in catalytic and process chemistry (*61*). Truly high-throughput embodiments of mini-ISES will likely require the development of appropriate robotic platforms and automation, for example, building around the proof-of-principle experiments demonstrated herein with the UV micromulticell. Future studies on the screening side will be directed at developing related platforms for an even more diverse array of chemical transformations. For, in the end, as Yoon and Jacobsen put it, "the identification of new 'privileged' ligands and catalysts remains enormously difficult and often requires a degree of serendipity (*64*)." It is hoped that the advances in both screening technology and ligand development described here will facilitate this enterprise.

MATERIALS AND METHODS

Experimental design

ISES is used here to provide useful estimates of relative reaction rate, substrate specificity, and % *ee* of an array of catalyst candidates in parallel. To obtain these data, the assay is performed in a biphasic system. The upper aqueous enzymatic reporting layer is positioned above the organic layer, and a UV/vis spectrophotometer is used to monitor the conversion of NAD to NADH in a semicontinuous fashion across multiple parallel cuvettes or wells, in using the micromulticell. The method requires that one identify a pair of screening enzymes that display distinct enantioselectivities for the chiral product being generated (1,2-propanediol and 1,2-hexanediol here). Toward this end, an array of KREDs (from Codexis, Sigma, Almac, or expressed in our laboratory) were screened, and four were selected as appropriate reporting enzymes for the screen. The enantioselectivity of these enzymes is described below. The miniaturized ISES procedure used for this work is outlined in detail after the enzyme characterization section. Finally, the second-generation synthesis of the carbafructopyranose diamine is reported, along with procedures to generate our best salen for this HKR and methods for its crystallization. This section concludes highlighting the HKR of *O*-phenylglycidol and 3-phenylpropylene oxide using this catalyst. Further synthetic detail for all compounds can be found in the Supplementary Materials.

KRED characterization

The enantioselectivity of each reporting enzyme was estimated by comparing the initial velocities of the oxidation for each (*R*) versus (*S*) product diols that would be obtained from the HKR of interest across a set of diol concentrations. Details can be found in the Supplementary Materials.

During earlier HKR-ISES experiments, we estimated the aqueous layer diol concentration to be in the range of 2.5 to 70 mM under screening conditions. Selectivity parameters appropriate for ISES screening are chosen on the basis of enantioselectivities observed in this concentration range. For KRED 119, a selectivity factor of 6.5 in favor of the (*R*)-1,2-hexanediol was used for ISES determinations. This corresponds to the selectivity observed in the standard assay cuvette at about 40 mM diol concentration. KRED 107 proved to be the most difficult reporting enzyme to parameterize, owing to its very high preference for the (*S*)-antipode of 1,2-hexanediol. In the end, iterative analysis of candidate fitting factors led us to assign a selectivity factor of 59 for this reporting enzyme (corresponds approximately to the selectivity of this reporting enzyme on the lower end of the aforementioned concentration window). Selectivity factors of 8.4 (v_S/v_R) for TBADH (*48*) and 6.5 (v_S/v_R) for KRED 23 were used for 1,2-propanediol reporting. The complete set of enantiomeric diol screening data (rate versus concentration) for each of the selected KRED screening enzymes is provided in the Supplementary Materials.

Procedure of the miniaturized ISES screen

Enzyme standardization.

Stock solutions: The following stock solutions were made for enzyme standardization: 40 mM β-$NADP^+$ (nicotinamide adenine dinucleotide phosphate), 130 mM β-NAD^+, TBADH (0.016 mg/μl), KRED 23 (0.016 mg/μl), KRED 107 (0.002 mg/μl), and KRED 119 (0.002 mg/μl) in 25 mM sodium phosphate buffer (pH 7.0), 2 M (*R*)-1,2-propanediol in water. Enzyme units were calculated by measuring the rate of formation of NADPH (reduced form of $NADP^+$) or NADH at 340 nm

(vide infra). In each case, one SI unit is taken as the amount of enzyme catalyzing the formation of NADPH (1 μmol/min).

Standardization of TBADH: The assay cuvette contained the following components: 2.2 mM (5 μl of 40 mM stock solution) β-$NADP^+$, 5 μl of TBADH stock solution, 71 μl of 50 mM sodium pyrophosphate buffer (pH 8.8), and 200 mM (9 μl of 2 M stock) (*R*)-1,2-propanediol. The reaction was initiated by the addition of the (*R*)-1,2-propanediol, which typically gave a rate of 0.709 abs/min at 25°C at 340-nm wavelength. This was indicative of 0.028 U/μl for the TBADH stock solution for the oxidation of (*R*)-1,2-propanediol.

Standardization of KRED 23: The assay cuvette contained the following components: 7.2 mM (5 μl of 130 mM stock solution) β-NAD^+, 5 μl of KRED 23 stock solution, 71 μl of 50 mM sodium pyrophosphate buffer (pH 8.8), and 200 mM (9 μl of 2 M stock) (*R*)-1,2-propanediol. The reaction was initiated by the addition of the (*R*)-1,2-propanediol, which typically gave a rate of 0.540 abs/min at 25°C at 340-nm wavelength. This is indicative of 0.016 U/μl for the KRED 23 stock solution for the oxidation of (*R*)-1,2-propanediol.

Standardization of KRED 107: The assay cuvette contained the following components: 2.2 mM (5 μl of 40 mM stock solution) β-$NADP^+$, 5 μl of KRED 107 stock solution, 81 μl of 50 mM sodium pyrophosphate buffer (pH 8.8), and 200 mM (9 μl of 2 M stock) (*R*)-1,2-hexanediol. The reaction was initiated by the addition of the (*R*)-1,2-hexanediol, which typically gave a rate of 0.124 abs/min at 25°C at 340-nm wavelength. This is indicative of 0.00398 U/μl for the KRED 107 stock solution for the oxidation of (*R*)-1,2-hexanediol.

Standardization of KRED 119: The assay cuvette contained the following components: 2.2 mM (5 μl of 40 mM stock solution) β-$NADP^+$, 5 μl of KRED 119 stock solution, 81 μl of 50 mM sodium pyrophosphate buffer (pH 8.8), and 200 mM (9 μl of 2 M stock) (*R*)-1,2-hexanediol. The reaction was initiated by the addition of the (*R*)-1,2-hexanediol, which typically gave a rate of 0.291 abs/min at 25°C at 340-nm wavelength. This was indicative of 0.00935 U/μl for the KRED 119 stock solution for the oxidation of (*R*)-1,2-hexanediol.

Layer composition. Quartz cuvettes with nominal 1-ml volumes were used in all previous ISES experiments. Here, we describe a general procedure using a 16 multimicrocell array for "cassette" ISES. For every catalyst, a four-well "cassette screen" was performed over the two different substrates: propylene oxide and hexene oxide. For propylene oxide, well A contains TBADH and well B contains KRED 23. For hexene oxide, well C contains KRED 107 and well D contains KRED 119. The organic layer in wells A and B had the following composition: 10 μl of propylene oxide (8.3 mg, 0.14 mmol), 10 μl of $CHCl_3$, and 0.25 mol % catalyst. The total organic layer volume was maintained at 20 μl. The organic layer in wells C and D had the following composition: 10 μl of hexene oxide (8.3 mg, 0.08 mmol), 10 μl of $CHCl_3$, and 0.25 mol % catalyst. The total organic layer volume was maintained at 20 μl. The aqueous layer in well A was 0.1 U of TBADH [3.6 μl from a stock solution (0.028 U/μl)], 2.2 mM β-$NADP^+$ (5 μl from a 40 mM stock solution), and 81.4 μl of 50 mM sodium pyrophosphate buffer, pH 8.8. The total volume of the aqueous layer was maintained at 90 μl. The aqueous layer in well B was 0.1 U of KRED 23 [6.2 μl from a stock solution (0.016 u/μl)], 7.2 mM β-NAD^+ (5 μl of 130 mM stock solution), and 78.8 μl of 50 mM sodium pyrophosphate buffer (pH 8.8). The total volume of the aqueous layer was maintained at 90 μl. The aqueous layer in well C was 0.0374 U of KRED 107 [9.4 μl from a stock solution (0.00398 U/μl)], 2.2 mM β-$NADP^+$ (5 μl from a 40 mM stock solution), and 75.6 μl of 50 mM sodium pyrophosphate buffer, pH 8.8. The total volume of the aqueous layer was maintained at 90 μl. The aqueous layer in well D was 0.0374 U of KRED 119 [4 μl from a stock solution (0.00935 U/μl)], 2.2 mM β-$NADP^+$ (5 μl from a 40 mM stock solution), and 81 μl of 50 mM sodium pyrophosphate buffer, pH 8.8. The total volume of the aqueous layer was maintained at 90 μl.

Step-by-step protocol. It was found to be practical to load the aqueous layers first. Routinely, 90-μl aqueous layers were loaded into individuate wells of 16-well quartz micromulticell either with a microsyringe or with a multichannel pipetter. The quartz cell was gently tapped to keep the layers evenly distributed in the solid quartz apparatus, and then cooled on ice. Then, the organic layers were prepared by briefly vortexing the catalyst stock in $CHCl_3$ with (±)-propylene oxide or (±)-hexene oxide in iced microcentrifuge tubes. The low-volume (20 μl) organic layer was then loaded to each well, most easily by rapidly syringing below the aqueous layer. For an example of the primary spectrophotometric data obtained, see the traces in Fig. 2 of the text (vide supra).

Synthesis of the β-D-carbafructopyranosyl-1,2-diamine

6-(Iodomethyl)-4-methoxy-2,2-dimethyltetrahydro-3aH-[1,3]dioxolo[4,5-c]pyran-7-ol (*21*). Methyl-α-D-mannopyranose (9 g, 46.3 mmol) was suspended in 200 ml of toluene at 80°C, and from that suspension, triphenylphosphine (13.9 g, 53.3 mmol) and imidazole (10.88 g, 160 mmol) were added, stirring continuously for 10 min at that temperature. Then, iodine (17.2 g, 66.7 mmol) was added in portions over 0.5 hour. The resulting suspension was vigorously stirred at 80°C for 2 hours, and solution became dark brown. The solution was cooled, the product was extracted into H_2O (3 × 200 ml), and the aqueous layer was washed with 200 ml of toluene and concentrated under vacuum. The crude was purified by column chromatography with pure ethyl acetate (R_f = 0.45 in 50% ethylacetate in acetone), and pure product (11.3 g, 80%) was obtained as white solid. $[\alpha]^{19}_D$ +64.3 (*c* 1.1, EtOH); ^{1}H NMR (nuclear magnetic resonance) (400 MHz, D_2O) δ 3.37 (dd, *J* = 10.9, 7.1 Hz, 1H), 3.45 (ddd, *J* = 9.4, 7.1, 2.2 Hz, 1H), 3.57 (app t, *J* = 9.5, 9.4 Hz, 1H), 3.63 (dd, *J* = 10.9, 2.2 Hz, 1H), 3.76 (dd, *J* = 9.5, 3.5 Hz, 1H), 3.93 (dd, *J* = 3.4, 1.7 Hz, 1H), 4.73 (d, *J* = 1.4 Hz, 1H); ^{13}C NMR (100 MHz, D_2O) δ 6.1, 55, 69.8, 70.05, 70.6, 71.5, 101.1; HMRS (FAB) calcd for $C_7H_{13}IO_5Li$ $(M + Li)^+$ 310.9968, obsd 310.9961.

6-(Iodomethyl)-4-methoxy-2,2-dimethyltetrahydro-3aH-[1,3]dioxolo[4,5-c]pyran-7-ol (*18*). To a solution of **21** (7.5 g, 24.6 mmol, 1 equivalent) in 120 ml of acetone at 0°C was added *p*-toluenesulfonic acid (936 mg, 4.92 mmol, 20%), followed by dropwise addition of dimethoxylpropane (9.1 ml, 73.8 mmol, 3 equivalent) via syringe pump. The resulting solution was continuously stirred for 3 hours, upon which time all the starting materials disappeared. The reaction was quenched by Et_3N (1.37 ml, 9.84 mmol, 40%), and organic solvent was evaporated under reduced pressure. The resulting residues were resuspended in 60 ml of water and extracted with EtOAc (3 × 60 ml). The organic layer was washed with brine and dried under Na_2SO_4, filtered and evaporated, and resulted in a pale yellowish liquid as clean product (8.5 g, 95%) without the need for further purification. $[\alpha]^{19}_D$ +33.4 (*c* 1.1, $CHCl_3$); ^{1}H NMR (400 MHz, $CDCl_3$) δ 1.34 (s, 3H), 1.51(s, 3H), 3.30 (dd, *J* = 10.5, 7.1 Hz, 1H), 3.4d (ddd, *J* = 9.2, 7.1, 2.4 Hz, 1H), 3.46 (s, 3H), 3.49 (ddd, *J* = 9.4, 6.9, 3.4 Hz 1H), 3.58(dd, *J* = 10.6, 2.5 Hz, 1H), 4.10 to 4.12 (m, 2H), 4.91 (s, 1H); ^{13}C NMR (100 MHz, $CDCl_3$) δ 6.81, 26.06, 27.97, 55,55, 68.95, 73.06, 75.69, 78.35, 98.33, 109.78; HMRS (FAB) calcd for $C_{10}H_{18}IO_5$ $(M + H)^+$ 345.0121, obsd 345.0204.

6-(Iodomethyl)-4,7-dimethoxy-2,2-dimethyltetrahydro-3aH-[1,3]dioxolo[4,5-c]pyran (*22*). To a solution of **18** (160 mg, 0.47 mmol) in 3 ml of THF at 0°C, imidazole (6.8 mg, 0.1 mmol) and NaH (240 mg, 60% suspension in mineral oil, 6 mmol) were added, followed by the slow addition of MeI (62 μl, 1 mmol). The resulting solution was continuously stirred at 0°C for 3 hours, upon which time thin-layer chromatography (TLC) showed complete consumption of the starting material. The reaction is quenched by saturated NH_4Cl and extracted with Et_2O. The organic phase was dried, filtered, and evaporated. The crude product was purified by silica column chromatography to afford **22** as a clear oil (134 mg, 80%). ^{1}H NMR (400 MHz, $CDCl_3$) δ 1.31 (s, 3H), 1.51 (s, 3H), 3.07 (dd, *J* = 9.6, 6.9 Hz, 1H), 3.27 (dd, *J* = 10.3, 7.4 Hz, 1H), 3.35 (ddd, *J* = 9.6, 7.4, 2.2 Hz, 1H), 3.43 (s, 3H), 3.50 (s, 3H), 4.06 (d, *J* = 5.7 Hz, 1H), 4.14 (app t, 1H); ^{13}C NMR (100 MHz, $CDCl_3$) δ 7.15, 26.18, 27.93, 55.91, 59.25, 67.91, 75.76, 78.09, 81.65, 98.21, 109.29; HRMS ESI calcd for $C_{11}H_{19}O_5INa$ $(M + Na)^+$ 381.0175, obsd 381.0164.

(3aR,4S,7S,7aR)-7-Hydroxy-4-methoxy-2,2-dimethyltetrahydrobenzo[d][1,3]dioxol-5(6H)-one (*19*). Two-step procedure from **18**: To 150 mg of **22** (0.42 mmol) in 5 ml of DMF, 0.7 ml DBU (0.46 mmol) was added at room temperature. The resulting mixture was stirred at 80°C overnight. The reaction mixture was cooled down, and 60 ml of EtOAc and 30 ml of saturated $NaHCO_3$ solution were added. The layers were separated, and the organic layer was washed with water (3 × 60 ml), and then with brine. The resulting organic phase was dried with Na_2SO_4 and evaporated under reduced pressure to give the product 60% yield: $[\alpha]^{19}_D$ +49.1 (*c* 1.1, $CHCl_3$); ^{1}H NMR (400 MHz, $CDCl_3$) δ 1.33 (s, 3H), 1.48 (s, 3H), 3.46 (d, *J* = 0.7 Hz, 3H), 3.49 (d, *J* = 0.7 Hz, 3H), 3.81 (dd, *J* = 0.8, 4.6 Hz, 1H), 4.16 (ddd, *J* = 7.2, 3.8, 0.5 Hz, 1H), 4.26 (dd, *J* = 7.1, 6.0 Hz, 1H), 4.43 (d, *J* = 0.8 Hz, 1H), 4.64 (d, *J* = 0.8 Hz, 1H), 4.86 (s, 1H); ^{13}C NMR (100 MHz, $CDCl_3$) δ 24.74, 26.89, 56.25, 57.91, 74.58, 75.86, 77.97, 93.22, 100.23, 109.80, 151.94; HMRS (FAB) calcd for $C_{11}H_{18}O_5Li$ $(M + Li)^+$ 237.031, obsd 237.1316. For the one-pot process: 1.3 g of **18** (3.78 mmol) was dissolved in 40 ml of DMF, cooled to 0°C, and 0.47 ml MeI (7.56 mmol) was added, followed by 51 mg of imidazole (0.76 mmol, 20%) and 272 mg of NaH (11.3 mmol, washed with hexane to remove mineral oil). The reaction mixture was continuously stirred at 0°C for 3 hours, and TLC shows all SM converted to alkene product and iodide intermediate. The reaction mixture was continuously stirred at room temperature overnight. TLC showed a single spot as the eliminated product. Workup: The reaction mixture was added 60 ml of EtOAc and 30 ml of saturated $NaHCO_3$ solution. The layers were separated, and the organic layer was washed with water (3 × 60 ml), and then with brine. The resulting organic phase was dried with Na_2SO_4 and evaporated under reduced pressure to give **19** as a colorless oil (0.85 g, 98%).

(3aR,4S,7S,7aR)-7-Hydroxy-4-methoxy-2,2-dimethyltetrahydrobenzo[d][1,3]dioxol-5(6H)-one (*20*). **19** (5.21 g, 22.6 mmol) was dissolved in 120 ml of solvent containing 2:2:1 volume ratio of acetone, dioxane, and H_2O. The solution was cooled to 0°C, and $Pd(OAc)_2$ (10 mol %) was added in portions. The reaction mixture was kept at 0°C for 12 hours, and the TLC showed complete consumption of the starting material. The reaction mixture was diluted with saturated NaCl and extracted with EtOAc (3 × 60 ml). The resulting organic phase was dried with Na_2SO_4, filtered, and evaporated under reduced pressure. The residue was purified by column chromatography (R_f = 0.25 at 50% EA in hexanes), and 4.15 g of product was obtained (85% total yield, which contains about 8% of the 5-epimer). For the major epimer: $[\alpha]^{19}_D$ −32.9 (*c* 1.0, $CHCl_3$); ^{1}H NMR (400 MHz, $CDCl_3$) δ 1.30 (s, 3H), 1.41 (s, 3H), 2.42 (dd, *J* = 18.3, 6.2 Hz, 1H), 2.75 (dd, *J* = 18.3, 5.0 Hz, 1H), 3.45 (s, 3H), 3.56 to 3.63 (m, 1H), 3.70 (d, *J* = 5.2 Hz, 1H), 4.27 (app t, *J* = 6.9, 5.4 Hz, 1H), 4.39 (dd, *J* = 7.0, 5.3 Hz, 1H), 5.51 to 5.55 (m, 2H); ^{13}C NMR (100 MHz, $CDCl_3$) δ 24.26, 26.73, 41.86, 59.00, 67.50, 76.71, 77.04, 83.89, 109.77, 204.70; HRMS FAB calcd for $C_{10}H_{17}O_5$ $(M + H)^+$ 217.1076, obsd 217.1073.

(3aR,4S,7aR)-4-Methoxy-2,2-dimethyl-3a,4-dihydrobenzo[*d*][1,3]dioxol-5(7aH)-one (*23*). To a solution of **20** (692 mg, 3.2 mmol) in 10 ml of CH_2Cl_2 at 0°C, diisopropyethyl amine (1.11 ml, 6.4 mmol) and 1 crystal of DMAP were added. Then, MsCl (371 μl, 4.8 mmol) was added dropwise, and the resulting solution was stirred at room temperature until SM disappeared. The reaction was quenched by the addition of saturated NH_4Cl and extracted with CH_2Cl_2; column chromatography purification afforded **23** as a clear oil (480 mg, 76% yield). $[\alpha]^{19}_D$ −84.4 (*c* 0.65, $CHCl_3$); ^{1}H NMR (400 MHz, $CDCl_3$) δ 1.35 (d, *J* = 4.26 Hz, 3H), 1.40 (d, *J* = 4.38 Hz, 3H), 3.45 (d, *J* = 4.5 Hz, 3H), 3.82 (app t, *J* = 4.4, 5.2 Hz, 1H), 4.47 (m, 1H), 4.73 (m, 1H), 5.99 (dd, *J* = 10.25, 4.53 Hz, 1H), 6.64 to 6.69 (m, 1H); ^{13}C NMR (100 MHz, $CDCl_3$) δ 26.29, 27.82, 59.17, 71.12, 76.68, 81.07, 110.96, 128.08, 143.32, 194.96; HRMS FAB calcd for $C_{10}H_{14}LiO_4$ $(M + Li)^+$ 205.1052, obsd 205.1046.

(3aR,4S,7aR)-4-Methoxy-2,2-dimethyltetrahydrobenzo[d][1,3]dioxol-5(6H)-one (*12*). To a solution of **23** (200 mg, 1.0 mmol) in EtOAc (10 ml) was added 20% $Pd(OH)_2$/C (20 wt%, 40 mg). The resulting mixture was hydrogenated at 20 psi for 1 hour, and the catalyst was then filtered off a pad of Celite and washed with EtOAc. The filtrate was evaporated to give the ketone **12** as a colorless oil (202 mg, 100% yield). $[\alpha]^{19}_D$ −69.6 (*c* 1.1, $CHCl_3$); ^{1}H NMR (400 MHz, $CDCl_3$) δ 1.33 (s, 3H), 1.43 (s, 3H), 2.09 to 2.14 (m, 1H), 2.21 to 2.30 (m, 2H), 2.46 to 2.55 (m, 1H), 3.41(s, 3H), 4.31 (dd, *J* = 6.8, 4.6 Hz, 1H), 4.41 to 4.48 (m, 1H); ^{13}C NMR (100 MHz, $CDCl_3$) δ 23,70, 24.38, 26.72, 32.68, 58.80, 72.29, 78.05, 84.23, 109.22, 207.53; HRMS (CI) calcd for $C_{11}H_{19}O_3$ $(M + H)^+$ 199.1334, obsd 199.1338.

(3aR,4R,7aR)-4-Methoxy-2,2-dimethyl-5-methylenehexahydrobenzo[d][1,3]dioxole (*13*). To a stirred ice-cold solution of Ph_3PCH_3Br (1.32 g, 2.14 mmol, 1.5 equivalent), 1.3 M BuLi in hexanes (1.5 ml, 2.0 mmol, 1.4 equivalent) was slowly added. The resulting yellow solution was stirred for 10 min at 0°C, and the ethereal solution of the ketone (288 mg, 1.44 mmol, 1 equivalent) was added slowly. Immediate precipitation appeared, and the resulting suspension was stirred overnight and quenched with 1 M NaOH. The product was extracted with ether, washed with brine, and dried over Na_2SO_4. Removal of solvent under reduced pressure provided the crude product. The product was purified by column chromatography on silica gel to yield the terminal olefin **9** (228 mg, 80%) as a clear liquid. $[\alpha]^{19}_D$ −96.2 (*c* 1.0, $CHCl_3$); ^{1}H NMR (400 MHz, CDCl3) δ 1.26 (d, *J* = 2.5 Hz, 3H), 1.41 (d, *J* = 2.6 Hz, 3H), 1.77 to 1.81 (m, 1H), 1.86 to 1.92 (m, 1H), 2.11 to 2.14 (m, 1H), 2.20 to 2.27 (m, 1H), 3.30 (d, *J* = 2.8 Hz, 3H), 3.61 (dt, *J* = 3.8, 1.1 Hz, 1H), 3.93 to 3.97 (m, 1H), 4.23 to 4.26 (m, 1H), 4.92 (d *J* = 1.08 Hz, 3H); ^{13}C NMR (100 MHz, $CDCl_3$) δ 25,32, 25.78, 26.15, 27.49, 57.25, 73.48, 79.43, 83.23, 108.18, 111.20, 142.53; HRMS (CI) calcd for $C_{11}H_{19}O_3$ $(M + H)^+$ 199.1334, obsd 199.1338.

(3aR,4R,5S,7aR)-5-Azido-5-(azidomethyl)-4-methoxy-2,2-dimethylhexahydro-benzo[d][1,3]dioxole (β-diazide) (*15*). A dry flask was charged with NaN_3 (442 mg, 6.8 mmol, 5 equivalent), Mn $(OAc)_3$-$2H_2O$ (1.1 g, 4.1 mmol, 3 equivalent), and CH_3CN (7 ml) and nitrogen gas were bubbled through the mixture. Then, the reaction mixture was cooled down to −20°C, and **13** (270 mg, 1.36 mmol,

1 equivalent) was added to it dropwise. The reaction was initiated by the slow addition of TFA (0.21 ml). The reaction mixture was slowly warmed up to room temperature. After 3 hours, aqueous $NaHSO_3$ solution was added, and the reaction mixture was extracted with CH_2Cl_2. The organic layer was washed with satd Na_2CO_3 and dried. Column chromatography (10% Et_2O in hexanes) gave two fractions with very close R_f values, with 80% yield. Fraction 1 yielded β-diazide **15** as a clear oil (84 mg, 22%); $[\alpha]^{19}_D$ −84.2 (*c* 1.05, $CHCl_3$); ^{1}H NMR (400 MHz, $CDCl_3$) δ 1.32 (s, 3H), 1.48 (s, 3H), 1.59 (m, 1H), 1.71 (dt, *J* = 14, 5.5 Hz, 1H), 1.92 (m, 2H), 3.22 (d, *J* = 7.3 Hz, 1H), 3.53(s, 3H), 3.55 (d, *J* = 12.1 Hz, 1H), 3.62 (d, *J* = 12.1 Hz, 1H), 4.13 (dd, *J* = 7.2, 5.4 Hz 1H), 4.25 (m, 1H); ^{13}C NMR (100 MHz, $CDCl_3$) δ 21.8, 26.2, 26.3, 28.4, 55.3, 60.2, 65.8, 73.9, 79.7, 82.5, 108.5; HRMS (FAB) calcd for $C_{13}H_{19}N_6O_3$ $(M + H)^+$ 283.1519, obsd 283.1530. Fraction 2 yielded the α-diazide **14** as a clear oil (221 mg, 58%); $[\alpha]^{19}_D$ −110.3 (*c* 1.0, $CHCl_3$); ^{1}H NMR (400 MHz, $CDCl_3$) δ 1.31 (s, 3H), 1.49 (s, 3H), 1.64 (m, 2H), 1.83 (m, 1H), 2.03 (m, 1H), 3.18 (d, *J* = 13.4 Hz, 1H), 3.35 (d, *J* = 7.1 Hz, 1H), 3.55 (s, 3H), 3.68 (d, *J* = 13.4 Hz, 1H), 3.90 (app t, *J* = 6.8 Hz, 1H), 4.21 (m, 1H); ^{13}C NMR (100 MHz, $CDCl_3$) δ 22.6, 25.4, 26.1, 28.2, 51.2, 60.4, 66.2, 73.3, 79.2, 85.2, 108.8; HRMS (FAB) calcd for $C_{11}H_{18}N_6O_3Li$ $(M + Li)^+$ 289.1600, obsd 289.1596.

(3aR,4R,5S,7aR)-5-(Aminomethyl)-4-methoxy-2,2-dimethylhexahydrobenzo-[*d*][1,3]dioxol-5-amine (β-diamine) (*17*). β-Diazide **15** (321 mg, 1.14 mmol) was dissolved in EtOH (10 ml), and 32 mg of 10% Pd/C was added. The resulting suspension was hydrogenated at 52 psi for 12 hours, resulting total reduction to give β-diamine **17** (262 mg, 100%). $[\alpha]^{19}_D$ −61.5 (*c* 0.76, $CHCl_3$); ^{1}H NMR (400 MHz, $CDCl_3$) δ 1.30 (br s, 4H), 1.33 (s, 3H), 1.5 (s, 3H), 1.54 (dt, *J* = 13.5, 4.6 Hz, 2H), 1.87 (br d, *J* = 13.2 Hz, 1H), 2.04 (tt, *J* = 13.3, 4.7 Hz, 1H), 2.6 (d, *J* = 12.7 Hz, 1H), 2.63 (d, *J* = 12.7 Hz, 1H), 3.08 (d, *J* = 7.2 Hz, 1H), 3.51 (s, 3H), 4.16 (app t, *J* = 6.8 Hz, 1H), 4.26 (m, 1H); ^{13}C NMR (100 MHz, $CDCl_3$) δ 21.9, 26.4, 27.7, 28.4, 51.7, 56.0, 60.0, 74.4, 80.2, 84.1, 107.7; HRMS (FAB) calcd for $C_{13}H_{23}N_2O_3$ $(M + H)^+$ 231.1709, obsd 231.1700.

α-Diamine (*16*). α-Diazide **14** (168 mg, 0.6 mmol) was dissolved in EtOH (5 ml), and 20 mg of 10% Pd/C was added. The resulting suspension was hydrogenated at 52 psi for 12 hours, resulting total reduction to give α-diamine **16** (135 mg, 100%). $[\alpha]^{19}_D$ −54.7 (*c* 0.35, $CHCl_3$); ^{1}H NMR (400 MHz, $CDCl_3$) δ 1.30 (br s, 3 H), 1.37 to 1.47 (m, 4 H), 1.48 (s, 3 H), 1.54 (dt, *J* = 13.6, 4 Hz, 1 H), 1.60 to 1.70 (m, 1 H), 1.92 (qt, *J* = 4, 15.6 Hz, 1 H), 2.42 (d, *J* = 13.2 Hz, 1 H), 2.67 (d, *J* = 13.2 Hz, 1 H), 3.14 (d, *J* = 7.2 Hz, 1 H), 3.51 (s, 3 H), 3.96 (dd, *J* = 5.6, 7.6 Hz, 1 H), 4.20 to 4.24 (m, 1 H); HRMS (ESI) calcd for $C_{13}H_{23}N_2O_3$ $(M + H)^+$ 231.1709, obsd 231.1706.

General procedure for the synthesis and crystallization of the Co(II)-salen complexes

Co(II)-**17c** used as an example: To an oven-dried round bottom flask, diamine **17** (65 mg, 0.28 mmol, 1 equivalent), 3,5-diiodosalicylaldehyde (190 mg, 0.51 mmol, 1.8 equivalent), and freshly distilled ethanol (3 ml) were added. The reaction mixture was heated at 50°C overnight. TLC indicated completion of the reaction. The reaction was concentrated in vacuo. The residue was purified by silica gel column chromatography (eluting with EtOAc/hexanes: 0 to 30%) to afford salen **17c** as a yellow solid (211 mg, 88%). $[\alpha]^{19}_D$ −138.4 (*c* 1.0, $CHCl_3$); ^{1}H NMR (400 MHz, CD_3Cl_3) δ 1.33 (s, 3H), 1.53 (s, 3H), 1.86 to 1.88 (m, 1H), 1.95 to 1.97 (m, 2H), 2.06 to 2.08 (m, 1H), 3.41 (d, *J* = 7.7 Hz, 3H), 3.59 (s, 3H), 3.98 (d, *J* = 12.5 Hz, 1H), 3.83 (d, *J* = 12.5 Hz, 1H), 4.8 (dd, *J* = 7.5, 5.4 Hz, 1H), 4.28 (br s, 1H), 7.48 (d, *J* = 1.9 Hz, 1H), 7.51 (d, *J* = 1.9 Hz, 1H), 8.04 (d, *J* = 1.9 Hz, 1H), 8.05 (d, *J* = 1.9 Hz, 1H), 8.12 (s, 1H), 8.37 (d, *J* = 1.73 Hz, 1H), 14.05 (s, 1H), 14.83 (s, 1H); ^{13}C NMR (100 MHz, CD_3Cl_3) δ 21.8, 26.3, 27.4, 28.4, 60.8, 63.9, 65.3, 73.7, 78.6, 79.3, 79.7, 83.9, 87.3, 88.9, 108.4, 119.4, 119.6, 139.9, 140.6, 149.0, 149.2, 160.3, 162.3, 163.8, 165.4; HMRS (FAB) calcd for $C_{25}H_{27}N_2O_5I_4$ $(M + H)^+$ 942.8021, obsd 942.8115.

The ligand **17c** (116 mg, 0.14 mmol, 1 equivalent) was dissolved in 1 ml CH_2Cl_2, and a methanolic (1 ml) solution of cobalt (II) acetate tetrahydrate (34 mg, 0.14 mmol, 1 equivalent) was added via cannula under Ar. The Co(II)-**17c** complex precipitated out after stirring for 30 min. After filtration, the solid was dried under vacuum to afford **17c** (102 mg, 68%) as a red solid.

A 1-dram vial was taken, and the inner walls were scratched with a glass pipette to get a visibly rough surface. This vial was charged with 15 mg of the Co(II)-**17c** complex, and about 1 ml of $CHCl_3$ was added to it. The contents were gently warmed in a ~ 60°C water bath to fully dissolve the solid. Methanol was slowly added at room temperature until the solution turned turbid. The mixture was heated again, and the solution became clear. The vial was capped and cooled down slowly. After 2 days, red crystals were harvested and sent for diffraction.

General procedure for HKR reactions using the Co(III)-17c catalyst

The Co(II)-**17c** complex was taken up in CH_2Cl_2 (2 ml) and stirred with 3,5-dinitrobenzoic acid (1 equivalent) in open air. The oxidation could be followed by TLC {formation of a greenish-brown spot of lower R_f [Co-(III) complex] from the visibly red, higher R_f spot characteristic of the Co(II)-**17c** salen}. When TLC indicated the completion of the reaction, the solvent was evaporated, and the Co(III)-**17c**-3,5-DNB complex was further dried in vacuo. The Co(III)-**17c** catalyst was used directly for HKR experiments, under ISES (biphasic) conditions or under typical neat or one-phase flask conditions.

Two different general procedures were adapted on the basis of the ease of handling of the epoxides (see the Supplementary Materials for a complete set of examples and characterization data). Representative examples are provided herewith.

Procedure A: 3-Phenoxy-1,2-epoxypropane (*O*-phenylglycidol)—HKR

Catalyst Co(III)-**17c**-3,5-DNB (5 mg, 0.005 mmol, 0.5 mol % loading) was mixed with 3-phenoxy-1,2-epoxypropane (150 mg, 1 mmol) and 300 μl of CH_2Cl_2. The mixture was cooled to 0°C, and the reaction was initiated by adding 9 μl (0.5 equivalent) of water, and stirring was continued for 20 hours at room temperature. After the reaction, silica gel column chromatography provided the unreacted 3-phenoxy-1,2-epoxypropane (71 mg, 47%, eluting with 50% ether/pentane) and 3-phenoxy-1,2-propanediol (*O*-phenylglycidol; 77 mg, 46%, further eluting with 10% methanol/ether).

3-Phenoxy-1,2-epoxypropane. ^{1}H NMR (400 MHz, $CDCl_3$) δ 2.73 to 2.79 (m, 1H), 2.89 to 2.91 (t, *J* = 4.8 Hz, 1H), 3.33 to 3.37 (m, 1H), 3.94 to 4.04 (m, 1H), 4.19 to 4.25 (m, 1H), 6.88 to 7.00 (m, 3H), 7.23 to 7.33 (m, 2H); $[\alpha]^{19}_D$ obsd +22.3 (for 96% *ee* of *S*), $[\alpha]^{19}_D$ +23.0, calcd (*c* = 1.4, $CHCl_3$). The enantiomers of this epoxide were resolved via HPLC (Chiralcel OD column). For the epoxide (hexanes/*i*-PrOH 87:13, flow rate 1 ml/min), minor isomer, t_R = 8.2 min (*R*) and major isomer, t_R = 12.4 min (*S*).

3-Phenoxy-1,2-propanediol. ^{1}H NMR (400 MHz, $CDCl_3$) δ 2.54 (br s, 1H), 3.03 (br s, 1H), 3.71 to 3.84 (m, 2H), 4.01 to 4.11 (m, 3H), 6.88 to 6.98 (m, 3H), 7.23 to 7.30 (m, 2H); $[\alpha]^{19}_D$ obsd −9.1 (for 92% *ee*

of *R*), $[\alpha]^{19}_{D}$ −9.9, calcd (*c* = 1.4, $CHCl_3$), [lit.(*110*) $[\alpha]^{23}_{D}$ −10.0 (*c* = 1.9, EtOH)]. The enantiomers of the diol were also resolved using a Chiralcel OD column. For the diol (hexanes/*i*-PrOH 90:10, flow rate 1 ml/min), major isomer, t_R = 15.6 min (*R*) and minor isomer, t_R = 33.7 min (*S*).

Procedure B: 1,2-Epoxy-3-phenylpropane—HKR

Starting from epoxy-3-phenylpropane (315 mg, 2.3 mmol), treatment with catalyst Co(III)-**17c**-3,5-DNB (24.8 mg, 0.023 mmol, 1 mol %) and 22 μl (0.5 equivalent) of water at 0°C over 12 hours resulted in 51% conversion as judged by ^{1}H NMR (small aliquot). The crude reaction mixture was then added to a freshly prepared solution of sodium phenylselenide, leading to direct epoxide ring opening with phenyl selenide anion. After workup and SiO_2 column chromatography, both the seleno-alcohol (329 mg, 48%, 0⟶50% ether in pentane) and 3-phenyl-1,2-propanediol (175 mg, 49%, 50⟶0% ether in EtOAc) were obtained.

1-(Phenylseleno)-3-phenyl-2-propanol. ^{1}H NMR (400 MHz, $CDCl_3$) δ 2.36 (d, *J* = 3.6 Hz, 1H), 2.86 to 2.88 (m, 2H), 2.91 to 2.96 (m, 1H), 3.10 to 3.14 (m, 1H), 3.92 to 3.96 (m, 1H), 7.17 to 7.30 (m, 8H), 7.47 to 7.50 (m, 2H); $[\alpha]^{19}_{obsd}$ −31.7 (for 97% *ee* of *R*), $[\alpha]^{19}_{D}$ −32.4, calcd (*c* = 1.0, $CHCl_3$). The seleno-alcohol was further derivatized using a classical Mosher ester procedure. The enantiomeric excess of the epoxide was subsequently estimated from integration of the methoxy groups on the two diastereomers (see the Supplementary Materials for detailed derivatization conditions and ^{1}H NMR of the two Mosher esters); major isomer, δ = 3.47 ppm (*R*) and minor isomer δ = 3.36 ppm (*S*).

3-Phenylpropane-1,2-diol. ^{1}H NMR (400 MHz, $CDCl_3$) δ 2.68 to 2.78 (m, 2H), 3.44 to 3.48 (m, 2H), 3.63 (d, *J* = 10.8 Hz, 2H), 3.89 (d, *J* = 5.6 Hz, 1H), 7.18 to 7.31 (m, 5H); $[\alpha]^{19}_{obsd}$ −21.5 (for 92% *ee* of *S*), $[\alpha]^{19}_{D}$ −23.3, calcd (*c* = 1.0, $CHCl_3$), [lit.(*134*) $[\alpha]_D$ −18.6 (*c* = 1.3, $CHCl_3$) for (*S*)-diol, lit.(*135*) $[\alpha]^{20}_{D}$ +20.4, (*c* = 1.0, $CHCl_3$) for (*R*)-diol, lit.(*136*) $[\alpha]^{20}_{D}$ +15.0, (*c* = 1.0, $CHCl_3$) for (*R*)-diol, lit. (*137*) $[\alpha]_D$ −29.0, (*c* = 1.2, EtOH) for (*S*)-diol]. The enantiopurity of the 1,2-diol was established by chiral HPLC (Chiralcel OD; hexane/i-PrOH 92:8, flow rate: 1 ml/min), minor isomer, t_R = 12.1 min (*R*) and major isomer, t_R = 13.2 min (*S*).

SUPPLEMENTARY MATERIALS

Supplementary material for this article is available at http://advances.sciencemag.org/cgi/content/full/1/6/e1500066/DC1

Complete description of ISES reporting enzymes; synthetic procedures and full spectral characterization for synthetic intermediates, chiral HPLC traces used to determine enantiopurity of all HKR products, step height analysis from the Co-salen x-ray crystal structures (93 pages).

Fig. S1. Enantioselectivity of the new KRED-119 reporting enzyme.

Fig. S2. Enantioselectivity of the new KRED-107 reporting enzyme.

Fig. S3. Enantioselectivity of the new KRED-23 reporting enzyme.

Fig. S4. Geometric parameters used to estimate step height for the carbafructopyranose-based Co-salen complexes.

Fig. S5. Step heights from x-ray crystal structures of the carbafructopyranose-based Co-salen complexes.

Table S1. HRMS characterization of Co(III)-salen catalysts.

Table S2. HKR under standard "round bottom flask conditions" with Co(III)-salen-3,5-DNB complexes.

REFERENCES AND NOTES

1. J. C. Ianni, V. Annamalai, P.-W. Phuan, M. Panda, M. C. Kozlowski, A priori theoretical prediction of selectivity in asymmetric catalysis: Design of chiral catalysts by using quantum molecular interaction fields. *Angew. Chem. Int. Ed.* **45**, 5502–5505 (2006).
2. M. C. Kozlowski, J. C. Ianni, Quantum molecular interaction field models of substrate enantioselection in asymmetric processes. *J. Mol. Catal. A Chem.* **324**, 141–145 (2010).
3. A. McNally, C. K. Prier, D. W. C. MacMillan, Discovery of an α-amino C–H arylation reaction using the strategy of accelerated serendipity. *Science* **334**, 1114–1117 (2011).
4. D. W. Robbins, J. F. Hartwig, A simple, multidimensional approach to high-throughput discovery of catalytic reactions. *Science* **333**, 1423–1427 (2011).
5. M. R. Friedfeld, M. Shevlin, J. M. Hoyt, S. W. Krska, M. T. Tudge, P. J. Chirik, Cobalt precursors for high-throughput discovery of base metal asymmetric alkene hydrogenation catalysts. *Science* **342**, 1076–1080 (2013).
6. W. Zhao, L. Huang, Y. Guan, W. D. Wulff, Three-component asymmetric catalytic Ugi reaction—Concinnity from diversity by substrate-mediated catalyst assembly. *Angew. Chem. Int. Ed.* **53**, 3436–3441 (2014).
7. F. Meng, K. P. McGrath, A. H. Hoveyda, Multifunctional organoboron compounds for scalable natural product synthesis. *Nature* **513**, 367–374 (2014).
8. H. Mandai, K. Mandai, M. L. Snapper, A. H. Hoveyda, Three-component Ag-catalyzed enantioselective vinylogous mannich and aza-Diels-Alder reactions with alkyl-substituted aldehydes. *J. Am. Chem. Soc.* **130**, 17961–17969 (2008).
9. J. Meeuwissen, J. N. H. Reek, Supramolecular catalysis beyond enzyme mimics. *Nat. Chem.* **2**, 615–621 (2010).
10. J. A. Kalow, A. G. Doyle, Enantioselective ring opening of epoxides by fluoride anion promoted by a cooperative dual-catalyst system. *J. Am. Chem. Soc.* **132**, 3268–3269 (2010).
11. S. Handa, V. Gnanadesikan, S. Matsunaga, M. Shibasaki, Heterobimetallic transition metal/rare earth metal bifunctional catalysis: A Cu/Sm/Schiff base complex for *syn*-selective catalytic asymmetric nitro-Mannich reaction. *J. Am. Chem. Soc.* **132**, 4925–4934 (2010).
12. C. E. Aroyan, M. M. Vasbinder, S. J. Miller, Dual catalyst control in the enantioselective intramolecular Morita–Baylis–Hillman reaction. *Org. Lett.* **7**, 3849–3851 (2005).
13. G. M. Sammis, H. Danjo, E. N. Jacobsen, Cooperative dual catalysis: Application to the highly enantioselective conjugate cyanation of unsaturated imides. *J. Am. Chem. Soc.* **126**, 9928–9929 (2004).
14. K. C. Harper, M. S. Sigman, Three-dimensional correlation of steric and electronic free energy relationships guides asymmetric propargylation. *Science* **333**, 1875–1878 (2011).
15. K. D. Collins, T. Gensch, F. Glorius, Contemporary screening approaches to reaction discovery and development. *Nat. Chem.* **6**, 859–871 (2014).
16. D. Leung, S. O. Kang, E. V. Anslyn, Rapid determination of enantiomeric excess: A focus on optical approaches. *Chem. Soc. Rev.* **41**, 448–479 (2012).
17. S. J. Taylor, J. P. Morken, Thermographic selection of effective catalysts from an encoded polymer-bound library. *Science* **280**, 267–270 (1998).
18. M. T. Reetz, M. H. Becker, K. M. Kuhling, A. Holzwarth, Time-resolved IR-thermographic detection and screening of enantioselectivity in catalytic reactions. *Angew. Chem. Int. Ed.* **37**, 2647–2650 (1998).
19. C. A. Evans, S. J. Miller, Proton-activated fluorescence as a tool for simultaneous screening of combinatorial chemical reactions. *Curr. Opin. Chem. Biol.* **6**, 333–338 (2002).
20. G. T. Copeland, S. J. Miller, A chemosensor-based approach to catalyst discovery in solution and on solid support. *J. Am. Chem. Soc.* **121**, 4306–4307 (1999).
21. V. I. Martin, J. R. Goodell, O. J. Ingham, J. A. Porco, A. B. Beeler, Multidimensional reaction screening for photochemical transformations as a tool for discovering new chemotypes. *J. Org. Chem.* **79**, 3838–3846 (2014).
22. J. L. Treece, J. R. Goodell, D. Vander Velde, J. A. Porco Jr., J. Aubé, Reaction discovery using microfluidic-based multidimensional screening of polycyclic iminium ethers. *J. Org. Chem.* **75**, 2028–2038 (2010).
23. P. W. Miller, L. E. Jennings, A. J. deMello, A. D. Gee, N. J. Long, R. Vilar, A microfluidic approach to the rapid screening of palladium-catalysed aminocarbonylation reactions. *Adv. Syn. Catal.* **351**, 3260–3268 (2009).
24. S. R. Stauffer, J. F. Hartwig, Fluorescence resonance energy transfer (FRET) as a high-throughput assay for coupling reactions. Arylation of amines as a case study. *J. Am. Chem. Soc.* **125**, 6977–6985 (2003).
25. S. H. Shabbir, C. J. Regan, E. V. Anslyn, A general protocol for creating high-throughput screening assays for reaction yield and enantiomeric excess applied to hydrobenzoin. *Proc. Natl. Acad. Sci. U.S.A.* **106**, 10487–10492 (2009).
26. R. Moreira, M. Havranek, D. Sames, New fluorogenic probes for oxygen and carbene transfer: A sensitive assay for single bead-supported catalysts. *J. Am. Chem. Soc.* **123**, 3927–3931 (2001).
27. K. Mikami, R. Angelaud, K. Ding, A. Ishii, A. Tanaka, N. Sawada, K. Kudo, M. Senda, Asymmetric activation of chiral alkoxyzinc catalysts by chiral nitrogen activators for dialkylzinc addition to aldehydes: Super high-throughput screening of combinatorial libraries of chiral ligands and activators by HPLC-CD/UV and HPLC-OR/RIU systems. *Chem. Eur. J.* **7**, 730–737 (2001).
28. J. R. Cabrera-Pardo, D. I. Chai, S. Liu, M. Mrksich, S. A. Kozmin, Label-assisted mass spectrometry for the acceleration of reaction discovery and optimization. *Nat. Chem.* **5**, 423–427 (2013).
29. J. Wassenaar, E. Jansen, W. J. van Zeist, F. M. Bickelhaupt, M. A. Siegler, A. L. Spek, J. N. Reek, Catalyst selection based on intermediate stability measured by mass spectrometry. *Nat. Chem.* **2**, 417–421 (2010).

30. C. Ebner, C. A. Müller, C. Markert, A. Pfaltz, Determining the enantioselectivity of chiral catalysts by mass spectrometric screening of their racemic forms. *J. Am. Chem. Soc.* **133**, 4710–4713 (2011).
31. C. A. Mueller, A. Pfaltz, Mass spectrometric screening of chiral catalysts by monitoring the back reaction of quasienantiomeric products: Palladium-catalyzed allylic substitution. *Angew. Chem. Int. Ed.* **47**, 3363–3366 (2008).
32. F. Bächle, J. Duschmalé, C. Ebner, A. Pfaltz, H. Wennemers, Organocatalytic asymmetric conjugate addition of aldehydes to nitroolefins: Identification of catalytic intermediates and the stereoselectivity-determining step by ESI-MS. *Angew. Chem. Int. Ed.* **52**, 12619–12623 (2013).
33. C. Mayer, D. Hilvert, A genetically encodable ligand for transfer hydrogenation. *Eur. J. Org. Chem.* **2013**, 3427–3430 (2013).
34. S. J. Zuend, M. P. Coughlin, M. P. Lalonde, E. N. Jacobsen, Scaleable catalytic asymmetric strecker syntheses of unnatural α-amino acids. *Nature* **461**, 968–970 (2009).
35. M. M. Müller, M. A. Windsor, W. C. Pomerantz, S. H. Gellman, D. Hilvert, A rationally designed aldolase foldamer. *Angew. Chem. Int. Ed.* **48**, 922–925 (2009).
36. N. Maillard, A. Clouet, T. Darbre, J.-L. Reymond, Combinatorial libraries of peptide dendrimers: Design, synthesis, on-bead high-throughput screening, bead decoding and characterization. *Nat. Protoc.* **4**, 132–142 (2009).
37. Y. Zhao, J. Rodrigo, A. H. Hoveyda, M. L. Snapper, Enantioselective silyl protection of alcohols catalyzed by an amino-acid-based small molecule. *Nature* **443**, 67–70 (2006).
38. G. Xu, S. R. Gilbertson, Development of building blocks for the synthesis of N-heterocyclic carbene ligands. *Org. Lett.* **7**, 4605–4608 (2005).
39. A. Berkessel, F. Cleemann, S. Mukherjee, Kinetic resolution of oxazinones: An organocatalytic approach to enantiomerically pure β-amino acids. *Angew. Chem. Int. Ed.* **44**, 7466–7469 (2005).
40. M. S. Sigman, E. N. Jacobsen, Schiff base catalysts for the asymmetric Strecker reaction identified and optimized from parallel synthetic libraries. *J. Am. Chem. Soc.* **120**, 4901–4902 (1998).
41. P. A. Lichtor, S. J. Miller, Experimental lineage and functional analysis of a remotely directed peptide epoxidation catalyst. *J. Am. Chem. Soc.* **136**, 5301–5308 (2014).
42. K. T. Barrett, A. J. Metrano, P. R. Rablen, S. J. Miller, Spontaneous transfer of chirality in an atropisomerically enriched two-axis system. *Nature* **509**, 71–75 (2014).
43. S. Han, S. J. Miller, Asymmetric catalysis at a distance: Catalytic, site-selective phosphorylation of teicoplanin. *J. Am. Chem. Soc.* **135**, 12414–12421 (2013).
44. E. A. Colby Davie, S. M. Mennen, Y. Xu, S. J. Miller, Asymmetric catalysis mediated by synthetic peptides. *Chem. Rev.* **107**, 5759–5812 (2007).
45. S. K. Ginotra, J. A. Friest, D. B. Berkowitz, Halocarbocyclization entry into the oxabicyclo [4.3.1]decyl exomethylene-δ-lactone cores of linearifolin and zaluzanin A: Exploiting combinatorial catalysis. *Org. Lett.* **14**, 968–971 (2012).
46. J. A. Friest, S. Broussy, W. J. Chung, D. B. Berkowitz, Combinatorial catalysis employing a visible enzymatic beacon in real time: Synthetically versatile (pseudo)halometalation/carbocyclizations. *Angew. Chem. Int. Ed.* **50**, 8895–8899 (2011).
47. S. Dey, D. R. Powell, C. Hu, D. B. Berkowitz, Cassette in situ enzymatic screening identifies complementary chiral scaffolds for hydrolytic kinetic resolution across a range of epoxides. *Angew. Chem. Int. Ed.* **46**, 7010–7014 (2007).
48. S. Dey, K. R. Karukurichi, W. Shen, D. B. Berkowitz, Double-cuvette ISES: In situ estimation of enantioselectivity and relative rate for catalyst screening. *J. Am. Chem. Soc.* **127**, 8610–8611 (2005).
49. D. B. Berkowitz, W. Shen, G. Maiti, In situ enzymatic screening (ISES) of P,N-ligands for Ni (0)-mediated asymmetric intramolecular allylic amination. *Tetrahedron Asymmetry* **15**, 2845–2851 (2004).
50. D. B. Berkowitz, G. Maiti, Following an ISES lead: The first examples of asymmetric Ni(0)-mediated allylic amination. *Org. Lett.* **6**, 2661–2664 (2004).
51. D. B. Berkowitz, M. Bose, S. Choi, In situ enzymatic screening (ISES): A tool for catalyst discovery and reaction development. *Angew. Chem. Int. Ed.* **41**, 1603–1607 (2002).
52. S. Kolodych, E. Rasolofonjatovo, M. Chaumontet, M.-C. Nevers, C. Créminon, F. Taran, Discovery of chemoselective and biocompatible reactions using a high-throughput immunoassay screening. *Angew. Chem. Int. Ed.* **52**, 12056–12060 (2013).
53. J. Quinton, S. Kolodych, M. Chaumonet, V. Bevilacqua, M. C. Nevers, H. Volland, S. Gabillet, P. Thuéry, C. Créminon, F. Taran, Reaction discovery by using a sandwich immunoassay. *Angew. Chem. Int. Ed.* **51**, 6144–6148 (2012).
54. J. Quinton, L. Charruault, M. C. Nevers, H. Volland, J. P. Dognon, C. Créminon, F. Taran, Toward the limits of sandwich immunoassay of very low molecular weight molecules. *Anal. Chem.* **82**, 2536–2540 (2010).
55. E. W. Debler, G. F. Kaufmann, M. M. Meijler, A. Heine, J. M. Mee, G. Pljevaljcic, A. J. Di Bilio, P. G. Schultz, D. P. Millar, K. D. Janda, I. A. Wilson, H. B. Gray, R. A. Lerner, Deeply inverted electron-hole recombination in a luminescent antibody-stilbene complex. *Science* **319**, 1232–1235 (2008).
56. A. Hamberg, S. Lundgren, M. Penhoat, C. Moberg, K. Hult, High-throughput enzymatic method for enantiomeric excess determination of O-acetylated cyanohydrins. *J. Am. Chem. Soc.* **128**, 2234–2235 (2006).
57. H. Matsushita, N. Yamamoto, M. M. Meijler, P. Wirsching, R. A. Lerner, M. Matsushita, K. D. Janda, Chiral sensing using a blue fluorescent antibody. *Mol. Biosyst.* **1**, 303–306 (2005).
58. C. M. Sprout, C. T. Seto, Using enzyme inhibition as a high throughput method to measure the enantiomeric excess of a chiral sulfoxide. *Org. Lett.* **7**, 5099–5102 (2005).
59. F. Taran, C. Gauchet, B. Mohar, S. Meunier, A. Valleix, P. Yves Renard, C. Créminon, J. Grassi, A. Wagner, C. Mioskowski, Communications: High-throughput screening of enantioselective catalysts by immunoassay. *Angew. Chem. Int. Ed.* **41**, 124–127 (2002).
60. P. Abato, C. T. Seto, EMDee: An enzymatic method for determining enantiomeric excess. *J. Am. Chem. Soc.* **123**, 9206–9207 (2001).
61. A. Buitrago Santanilla, E. L. Regalado, T. Pereira, M. Shevlin, K. Bateman, L.-C. Campeau, J. Schneeweis, S. Berritt, Z.-C. Shi, P. Nantermet, Y. Liu, R. Helmy, C. J. Welch, P. Vachal, I. W. Davies, T. Cernak, S. D. Dreher, Nanomole-scale high-throughput chemistry for the synthesis of complex molecules. *Science* **347**, 49–53 (2015).
62. K. M. Kuhn, J.-B. Bourg, C. K. Chung, S. C. Virgil, R. H. Grubbs, Effects of NHC-backbone substitution on efficiency in ruthenium-based olefin metathesis. *J. Am. Chem. Soc.* **131**, 5313–5320 (2009).
63. J. B. Matson, S. C. Virgil, R. H. Grubbs, Pulsed-addition ring-opening metathesis polymerization: Catalyst-economical syntheses of homopolymers and block copolymers. *J. Am. Chem. Soc.* **131**, 3355–3362 (2009).
64. T. P. Yoon, E. N. Jacobsen, Privileged chiral catalysts. *Science* **299**, 1691–1693 (2003).
65. J. Wassenaar, J. N. H. Reek, Hybrid bidentate phosphorus ligands in asymmetric catalysis: Privileged ligand approach vs. combinatorial strategies. *Org. Biomol. Chem.* **9**, 1704–1713 (2011).
66. A. Miyashita, A. Yasuda, H. Takaya, K. Toriumi, T. Ito, T. Souchi, R. Noyori, Synthesis of 2,2'-bis (diphenylphosphino)-1,1'-binaphthyl (BINAP), an atropisomeric chiral bis(triaryl)phosphine, and its use in the rhodium(I)-catalyzed asymmetric hydrogenation of .alpha.-(acylamino) acrylic acids. *J. Am. Chem. Soc.* **102**, 7932–7934 (1980).
67. D. B. Guthrie, D. P. Curran, Asymmetric radical and anionic cyclizations of axially chiral carbamates. *Org. Lett.* **11**, 249–251 (2008).
68. P. J. Pye, K. Rossen, R. A. Reamer, N. N. Tsou, R. P. Volante, P. J. Reider, A new planar chiral bisphosphine ligand for asymmetric catalysis: Highly enantioselective hydrogenations under mild conditions. *J. Am. Chem. Soc.* **119**, 6207–6208 (1997).
69. A. Togni, C. Breutel, A. Schnyder, F. Spindler, H. Landert, A. Tijani, A novel easily accessible chiral ferrocenyldiphosphine for highly enantioselective hydrogenation, allylic alkylation, and hydroboration reactions. *J. Am. Chem. Soc.* **116**, 4062–4066 (1994).
70. G. C. Fu, Applications of planar-chiral heterocycles as ligands in asymmetric catalysis. *Acc. Chem. Res.* **39**, 853–860 (2006).
71. G. C. Fu, Enantioselective nucleophilic catalysis with "planar-chiral" heterocycles. *Acc. Chem. Res.* **33**, 412–420 (2000).
72. N. Takenaka, J. Chen, B. Captain, R. S. Sarangthem, A. Chandrakumar, Helical chiral 2-aminopyridinium ions: A new class of hydrogen bond donor catalysts. *J. Am. Chem. Soc.* **132**, 4536–4537 (2010).
73. M. J. Narcis, N. Takenaka, Helical-chiral small molecules in asymmetric catalysis. *Eur. J. Org. Chem.* **2014**, 21–34 (2014).
74. T. Inoue, D. Sato, K. Komura, S. Itsuno, Enantiometrically pure 2-piperazinemethanols as novel chiral ligands of oxazaborolidine catalysts in enantioselective borane reductions. *Tetrahedron Lett.* **40**, 5379–5382 (1999).
75. E. J. Corey, C. J. Helal, Reduction of carbonyl compounds with chiral oxazaborolidine catalysts: A new paradigm for enantioselective catalysis and a powerful new synthetic method. *Angew. Chem. Int. Ed.* **37**, 1986–2012 (1998).
76. T. P. Pathak, S. J. Miller, Chemical tailoring of teicoplanin with site-selective reactions. *J. Am. Chem. Soc.* **135**, 8415–8422 (2013).
77. J. L. Gustafson, D. Lim, S. J. Miller, Dynamic kinetic resolution of biaryl atropisomers via peptide-catalyzed asymmetric bromination. *Science* **328**, 1251–1255 (2010).
78. K. W. Fiori, A. L. A. Puchlopek, S. J. Miller, Enantioselective sulfonylation reactions mediated by a tetrapeptide catalyst. *Nat. Chem.* **1**, 630–634 (2009).
79. C. A. Lewis, S. J. Miller, Site-selective derivatization and remodeling of erythromycin a by using simple peptide-based chiral catalysts. *Angew. Chem. Int. Ed.* **45**, 5616–5619 (2006).
80. A. Martinez, M. van Gemmeren, B. List, Unexpected beneficial effect of *ortho*-substituents on the (*S*)-proline-catalyzed asymmetric aldol reaction of acetone with aromatic aldehydes. *Synlett* **25**, 961–964 (2014).
81. V. Bisai, A. Bisai, V. K. Singh, Enantioselective organocatalytic aldol reaction using small organic molecules. *Tetrahedron* **68**, 4541–4580 (2012).
82. H. Yang, R. G. Carter, Synthesis of all-carbon, quaternary center-containing cyclohexenones through an organocatalyzed, multicomponent coupling. *Org. Lett.* **12**, 3108–3111 (2010).
83. H. Xie, L. Zu, H. Li, J. Wang, W. Wang, Organocatalytic enantioselective cascade Michael-alkylation reactions: Synthesis of chiral cyclopropanes and investigation of unexpected

organocatalyzed stereoselective ring opening of cyclopropanes. *J. Am. Chem. Soc.* **129**, 10886–10894 (2007).
84. K. R. Knudsen, C. E. T. Mitchell, S. V. Ley, Asymmetric organocatalytic conjugate addition of malonates to enones using a proline tetrazole catalyst. *Chem. Commun.*, 66–68 (2006).
85. D. D. Steiner, N. Mase, C. F. Barbas III, Direct asymmetric α-fluorination of aldehydes. *Angew. Chem. Int. Ed.* **44**, 3706–3710 (2005).
86. D. Enders, C. Grondal, M. Vrettou, G. Raabe, Asymmetric synthesis of selectively protected amino sugars and derivatives by a direct organo-catalytic Mannich reaction. *Angew. Chem. Int. Ed.* **44**, 4079–4083 (2005).
87. S. P. Brown, M. P. Brochu, C. J. Sinz, D. W. C. MacMillan, The direct and enantioselective organocatalytic α-oxidation of aldehydes. *J. Am. Chem. Soc.* **125**, 10808–10809 (2003).
88. K. B. Sharpless, Searching for new reactivity (Nobel lecture). *Angew. Chem. Int. Ed.* **41**, 2024–2032 (2002).
89. M. J. O'Donnell, The enantioselective synthesis of α-amino acids by phase-transfer catalysis with achiral Schiff base esters. *Acc. Chem. Res.* **37**, 506–517 (2004).
90. B. Lygo, B. I. Andrews, Asymmetric phase-transfer catalysis utilizing chiral quaternary ammonium salts: Asymmetric alkylation of glycine imines. *Acc. Chem. Res.* **37**, 518–525 (2004).
91. E. J. Corey, F. Xu, M. C. Noe, A rational approach to catalytic enantioselective enolate alkylation using a structurally rigidified and defined chiral quaternary ammonium salt under phase transfer conditions. *J. Am. Chem. Soc.* **119**, 12414–12415 (1997).
92. Y.-H. Lam, K. N. Houk, How cinchona alkaloid-derived primary amines control asymmetric electrophilic fluorination of cyclic ketones. *J. Am. Chem. Soc.* **136**, 9556–9559 (2014).
93. B. Mohar, J. Baudoux, J.-C. Plaquevent, D. Cahard, Electrophilic fluorination mediated by cinchona alkaloids: Highly enantioselective synthesis of α-fluoro-α-phenylglycine derivatives. *Angew. Chem. Int. Ed.* **40**, 4214–4216 (2001).
94. P. R. Carlier, W. S. Mungall, G. Schroder, K. B. Sharpless, Enhanced kinetic resolution and enzyme-like shape selectivity. *J. Am. Chem. Soc.* **110**, 2978–2979 (1988).
95. D. Seebach, A. K. Beck, A. Heckel, TADDOLs, their derivatives, and TADDOL analogs: Versatile chiral auxiliaries. *Angew. Chem. Int. Ed.* **40**, 92–138 (2001).
96. B. E. Evans, K. E. Rittle, M. G. Bock, R. M. DiPardo, R. M. Freidinger, W. L. Whitter, G. F. Lundell, D. F. Veber, P. S. Anderson, R. S. Chang, V. J. Lotti, D. J. Cerino, T. B. Chen, P. J. Kling, K. A. Kunkel, J. P. Springer, J. Hirshfield, Methods for drug discovery: Development of potent, selective, orally effective cholecystokinin antagonists. *J. Med. Chem.* **31**, 2235–2246 (1988).
97. M. E. Welsch, S. A. Snyder, B. R. Stockwell, Privileged scaffolds for library design and drug discovery. *Curr. Opin. Chem. Biol.* **14**, 347–361 (2010).
98. K. Barry Sharpless, W. Amberg, Y. L. Bennani, G. A. Crispino, J. Hartung, K. Sung Jeong, H. Lun Kwong, K. Morikawa, Z. Min Wang, The osmium-catalyzed asymmetric dihydroxylation: A new ligand class and a process improvement. *J. Org. Chem.* **57**, 2768–2771 (1992).
99. B. M. Trost, R. C. Bunt, R. C. Lemoine, T. L. Calkins, Dynamic kinetic asymmetric transformation of diene monoepoxides: A practical asymmetric synthesis of vinylglycinol, vigabatrin, and ethambutol. *J. Am. Chem. Soc.* **122**, 5968–5976 (2000).
100. M. Giannerini, M. Fañanás-Mastral, B. L. Feringa, *Z*-Selective copper-catalyzed asymmetric allylic alkylation with grignard reagents. *J. Am. Chem. Soc.* **134**, 4108–4111 (2012).
101. M. Fañanás-Mastral, M. Pérez, P. H. Bos, A. Rudolph, S. R. Harutyunyan, B. L. Feringa, Enantioselective synthesis of tertiary and quaternary stereogenic centers: Copper/phosphoramidite-catalyzed allylic alkylation with organolithium reagents. *Angew. Chem. Int. Ed.* **51**, 1922–1925 (2012).
102. J. F. Teichert, B. L. Feringa, Phosphoramidites: Privileged ligands in asymmetric catalysis. *Angew. Chem. Int. Ed.* **49**, 2486–2528 (2010).
103. S. T. Madrahimov, J. F. Hartwig, Origins of enantioselectivity during allylic substitution reactions catalyzed by metallacyclic iridium complexes. *J. Am. Chem. Soc.* **134**, 8136–8147 (2012).
104. D. Marković, J. F. Hartwig, Resting state and kinetic studies on the asymmetric allylic substitutions catalyzed by iridium–phosphoramidite complexes. *J. Am. Chem. Soc.* **129**, 11680–11681 (2007).
105. C. A. Kiener, C. Shu, C. Incarvito, J. F. Hartwig, Identification of an activated catalyst in the iridium-catalyzed allylic amination and etherification. Increased rates, scope, and selectivity. *J. Am. Chem. Soc.* **125**, 14272–14273 (2003).
106. For a recent discussion of the development of enantioselective, yet non-C_2-symmetric ligands, see: B. M. Trost, E. J. Donckele, D. A. Thaisrivongs, M. Osipov, J. T. Masters, A new class of non-C_2-symmetric ligands for oxidative and redox-neutral palladium-catalyzed asymmetric allylic alkylations of 1,3-diketones. *J. Am. Chem. Soc.* **137**, 2776–2784 (2015).
107. D. D. Ford, L. P. C. Nielsen, S. J. Zuend, E. N. Jacobsen, Mechanistic basis for high stereoselectivity and broad substrate scope in the (salen)Co(III)-catalyzed hydrolytic kinetic resolution. *J. Am. Chem. Soc.* **135**, 15595–15608 (2013).
108. L. P. C. Nielsen, S. J. Zuend, D. D. Ford, E. N. Jacobsen, Mechanistic basis for high reactivity of (salen)Co-OTs in the hydrolytic kinetic resolution of terminal epoxides. *J. Org. Chem.* **77**, 2486–2495 (2012).
109. L. P. C. Nielsen, C. P. Stevenson, D. G. Blackmond, E. N. Jacobsen, Mechanistic investigation leads to a synthetic improvement in the hydrolytic kinetic resolution of terminal epoxides. *J. Am. Chem. Soc.* **126**, 1360–1362 (2004).
110. S. E. Schaus, B. D. Brandes, J. F. Larrow, M. Tokunaga, K. B. Hansen, A. E. Gould, M. E. Furrow, E. N. Jacobsen, Highly selective hydrolytic kinetic resolution of terminal epoxides catalyzed by chiral (salen) Co^{III} complexes. Practical synthesis of enantioenriched terminal epoxides and 1, 2-diols. *J. Am. Chem. Soc.* **124**, 1307–1315 (2002).
111. M. M. Midland, J. I. McLoughlin, Asymmetric reduction of prochiral ketones with B-3-pinanyl-9-borabicyclo[3.3.1]nonane in efficiencies approaching 100%. Simultaneous rate enhancement and side reaction suppression via the use of elevated pressures. *J. Org. Chem.* **49**, 1316–1317 (1984).
112. H. C. Brown, P. V. Ramachandran, Versatile α-pinene-based borane reagents for asymmetric syntheses. *J. Organomet. Chem.* **500**, 1–19 (1995).
113. T. V. RajanBabu, A. L. Casalnuovo, Role of electronic asymmetry in the design of new ligands: The asymmetric hydrocyanation reaction. *J. Am. Chem. Soc.* **118**, 6325–6326 (1996).
114. Z.-X. Wang, Y. Tu, M. Frohn, J.-R. Zhang, Y. Shi, An efficient catalytic asymmetric epoxidation method. *J. Am. Chem. Soc.* **119**, 11224–11235 (1997).
115. Y. Shi, Organocatalytic asymmetric epoxidation of olefins by chiral ketones. *Acc. Chem. Res.* **37**, 488–496 (2004).
116. T. K. M. Shing, Y. Tang, A new approach to pseudo-sugars from (–)-quinic acid: Facile syntheses of pseudo-β-D-mannopyranose and pseudo-β-D-fructopyranose. *J. Chem. Soc. Chem. Commun.*, 748 (1990).
117. B. B. Snider, H. Lin, An improved procedure for the conversion of alkenes and glycals to 1,2-diazides using $Mn(OAc)_3$-$2H_2O$ in acetonitrile containing trifluoroacetic acid. *Syn. Commun.* **28**, 1913–1922 (1998).
118. X. Hong, M. Mellah, E. Schulz, Heterobimetallic dual-catalyst systems for the hydrolytic kinetic resolution of terminal epoxides. *Catal. Sci. Technol.* **4**, 2608–2617 (2014).
119. M. T. Reetz, M. Bocola, L. W. Wang, J. Sanchis, A. Cronin, M. Arand, J. Zou, A. Archelas, A. L. Bottalla, A. Naworyta, S. L. Mowbray, Directed evolution of an enantioselective epoxide hydrolase: Uncovering the source of enantioselectivity at each evolutionary stage. *J. Am. Chem. Soc.* **131**, 7334 (2009).
120. M. T. Reetz, H. Zheng, Manipulating the expression rate and enantioselectivity of an epoxide hydrolase by using directed evolution. *ChemBioChem* **12**, 1529–1535 (2011).
121. Å. J. Carlsson, P. Bauer, H. Ma, M. Widersten, Obtaining optical purity for product diols in enzyme-catalyzed epoxide hydrolysis: Contributions from changes in both enantio- and regioselectivity. *Biochemistry* **51**, 7627–7637 (2012).
122. C. L. Perrin, K. B. Armstrong, M. A. Fabian, The origin of the anomeric effect: Conformational analysis of 2-methoxy-1, 3-dimethylhexahydropyrimidine. *J. Am. Chem. Soc.* **116**, 715–722 (1994).
123. A recent computational study employing an extended block-localized wavefunction method lends support to the notion that the anomeric effect is dominated by electrostatic effects, e.g. dipole-dipole interactions: Y. Mo, Computational evidence that hyperconjugative interactions are not responsible for the anomeric effect. *Nat. Chem.* **2**, 666–671 (2010).
124. J. A. Kanters, G. Roelofsen, B. P. Alblas, I. Meinders, The crystal and molecular structure of β-D-fructose, with emphasis on anomeric effect and hydrogen-bond interactions. *Acta Cryst.* **B33**, 665–672 (1977).
125. A. Kwiecień, K. Ślepokura, T. Lis, Crystal structure of β-D-psicopyranose. *Carbohydr. Res.* **343**, 2336–2339 (2008).
126. S. Takagi, R. D. Rosenstein, Structure of α-D-tagatose and comparison with crystal structures of other ketohexoses. *Carbohydr. Res.* **11**, 156–158 (1969).
127. S. H. Kim, R. D. Rosenstein, Crystal structure of α-L-sorbose. *Acta Cryst.* **22**, 648–656 (1967).
128. K. Sun, W.-X. Li, Z. Feng, C. Li, Cooperative activation in ring-opening hydrolysis of epoxides by Co-salen complexes: A first principle study. *Chem. Phys. Lett.* **470**, 259–263 (2009).
129. R. Bobb, G. Alhakimi, L. Studnicki, A. Lough, J. Chin, Stereoselective recognition of an aziridine with a Co(III) complex: A potential transition-state analogue for catalytic epoxidation. *J. Am. Chem. Soc.* **124**, 4544–4545 (2002).
130. U. Arnold, B. R. Huck, S. H. Gellman, R. T. Raines, Protein prosthesis: β-Peptides as reverse-turn surrogates. *Protein Sci.* **22**, 274–275 (2013).
131. U. Arnold, M. P. Hinderaker, B. L. Nilsson, B. R. Huck, S. H. Gellman, R. T. Raines, Protein prosthesis: A semisynthetic enzyme with a β-peptide reverse turn. *J. Am. Chem. Soc.* **124**, 8522–8523 (2002).
132. C. E. Jakobsche, G. Peris, S. J. Miller, Functional analysis of an aspartate-based epoxidation catalyst with amide-to-alkene peptidomimetic catalyst analogues. *Angew. Chem. Int. Ed.* **47**, 6707–6711 (2008).
133. M. M. Vasbinder, E. R. Jarvo, S. J. Miller, Incorporation of peptide isosteres into enantioselective peptide-based catalysts as mechanistic probes. *Angew. Chem. Int. Ed.* **40**, 2824–2827 (2001).
134. A. Córdova, H. Sundén, A. Bøgevig, M. Johansson, F. Himo, The direct catalytic asymmetric α-aminooxylation reaction: Development of stereoselective routes to 1,2-diols and 1,2-amino alcohols and density functional calculations. *Chem. Eur. J.* **10**, 3673–3684 (2004).

135. M. Kapur, A. Khartulyari, M. E. Maier, Stereoselective synthesis of protected 1,2-diols and 1,2,3-triols by a tandem hydroboration–coupling sequence. *Org. Lett.* **8**, 1629–1632 (2006).
136. D. B. Ramachary, C. F. Barbas III, Direct amino acid-catalyzed asymmetric desymmetrization of *meso*-compounds: Tandem aminoxylation/O–N bond heterolysis reactions. *Org. Lett.* **7**, 1577–1580 (2005).
137. I. Ibrahem, G.-L. Zhao, H. Sundén, A. Córdova, A route to 1,2-diols by enantioselective organocatalytic α-oxidation with molecular oxygen. *Tetrahedron Lett.* **47**, 4659–4663 (2006).

Acknowledgments: We thank D. R. Powell (University of Oklahoma) for x-ray crystal structure determination. This research was facilitated by the IR/D (Individual Research and Development) program associated with D.B.B.'s appointment at the NSF. **Funding:** The authors thank the NSF (DMR-1214019) for support of this research and the NIH (SIG-1-510-RR-06307) and NSF (CHE-0091975, MRI-0079750) for NMR instrumentation support and the NIH (RR016544) for facilities renovation. **Author contributions:** K.R.K., X.F., R.A.S., S.B., W.S., S.D., and S.K.R. performed the experiments. This team, along with D.B.B., designed the experiments and interpreted the results. D.B.B., X.F., and R.A.S. wrote the manuscript. **Competing interests:** The authors declare that they have no competing interests. **Data and materials availability:** Coordinates for crystal structures of the following Co-salen complexes—Co(II)-**6a**, Co(II)-**6c**, and Co(II)-**17c**—will be deposited in the Cambridge Crystallographic Database.

Submitted 18 January 2015
Accepted 11 May 2015
Published 10 July 2015
10.1126/sciadv.1500066

Citation: K. R. Karukurichi, X. Fei, R. A. Swyka, S. Broussy, W. Shen, S. Dey, S. K. Roy, D. B. Berkowitz, Mini-ISES identifies promising (Carba)fructopyranose-based salens for asymmetric catalysis: Tuning ligand shape via the anomeric effect. *Sci. Adv.* **1**, e1500066 (2015).